OFDM with Index Modulation-Based Alternative Waveform Designs for Future Wireless Systems

by

Ömer Furkan Tuğtekin

A Dissertation Submitted to the
Graduate School of Sciences and Engineering
in Partial Fulfillment of the Requirements for
the Degree of

Master of Science

in

Electrical and Electronics Engineering

KOÇ ÜNİVERSİTESİ

September 12, 2022

OFDM with Index Modulation-Based
Alternative Waveform Designs for Future Wireless Systems

Koç University
Graduate School of Sciences and Engineering
This is to certify that I have examined this copy of a master's thesis by

Ömer Furkan Tuğtekin

and have found that it is complete and satisfactory in all respects,
and that any and all revisions required by the final
examining committee have been made.

Committee Members:

Assoc. Prof. Ertuğrul Başar (Advisor)

Prof. Sinem Çöleri

Assoc. Prof. Erdoğan Aydın

Date:

To my dear mother and father,

ABSTRACT

OFDM with Index Modulation-Based
Alternative Waveform Designs for Future Wireless Systems
Ömer Furkan Tuğtekin
Master of Science in Electrical and Electronics Engineering
September 12, 2022

Orthogonal frequency division multiplexing with index modulation (OFDM-IM), which transmits information bits through ordinary signal constellation symbols and indices of active subcarriers, is a promising multicarrier transmission scheme and has attracted the attention of researchers due to its several benefits such as flexibility and simplicity. Nonetheless, OFDM-IM cannot satisfy many needs of future wireless communication services such as, ultra-reliable low-latency communications (URLLC) and enhanced mobile broadband (eMBB) since providing superior reliability, high data rates, and low complexity is challenging due to its null subcarriers and unsufficient error performance. Therefore, several novel waveforms have been proposed by utilizing the flexible nature of the OFDM-IM to meet the diverse needs of eMBB and URRLC services. In this thesis, two novel OFDM-IM based multicarrier transmission schemes have been proposed by utilizing the aforementioned advantages of OFDM-IM.

Firstly, a novel transmission scheme named as coordinate interleaved OFDM with power distribution IM (CI-OFDM-PIM), which applies coordinate interleaving and power distribution in subcarriers to achieve a diversity gain that is equal to the number of subcarriers in a subblock, is proposed. The average bit error probability (ABEP) for the CI-OFDM-PIM was derived and the superior error performance of the proposed scheme over benchmarks has been shown via computer simulations.

Next, a novel OFDM-IM based scheme called coordinate interleaved OFDM with repeated in phase/quadrature IM (CI-OFDM-RIQIM), which provides superior error performance and enhanced spectral efficiency due to its diversity order of two and clever subcarrier activation pattern (SAP) detection mechanism, is proposed. Furthermore, a log-likelihood ratio (LLR) based low-complexity detector is designed for the proposed scheme. Theoretical analyses are performed and an upper bound on the bit error probability is derived. Comprehensive computer simulations under perfect and imperfect channel state information (CSI), are conducted to compare the proposed and reference schemes. It is shown that CI-OFDM-RIQIM shows superior results and can be considered as a promising candidate for next generation wireless communication systems.

ÖZETÇE

Geleceğin Kablosuz Sistemleri için İndis Modülasyonlu OFDM Tabanlı Alternatif Dalga Formu Tasarımları
Ömer Furkan Tuğtekin
Elektrik ve Elektronik Mühendisliği, Yüksek Lisans
12 Eylül 2022

Klasik sinyal kümesi sembolleri ve aktif alt taşıyıcıların indisleri aracılığıyla bilgi bitlerini ileten indis modülasyonlu dik frekans bölmeli çoğullama (orthogonal frequency division multiplexing with index modulation, OFDM-IM), umut verici bir çok taşıyıcılı iletim şemasıdır ve esneklik ve basitlik gibi çeşitli faydaları sayesinde araştırmacıların dikkatini çekmiştir. Bununla birlikte, OFDM-IM'in boş alt taşıyıcıları ve yetersiz hata performansından dolayı üstün güvenilirlik, yüksek veri hızları ve düşük karmaşıklık sağlayamaması aşırı güvenilir düşük gecikmeli iletişim (ultra-reliable low-latency communications, URLLC) ve gelişmiş mobil geniş bant (enhanced mobile broadband, eMBB) gibi geleceğin kablosuz iletişim hizmetlerinin birçok ihtiyacını karşılayamamasına sebep olmaktadır. Bu nedenle, eMBB ve URLLC hizmetlerinin çeşitli ihtiyaçlarını karşılamak için OFDM-IM'in esnek doğası kullanılarak birçok özgün dalga formu önerilmiştir. Bu tezde, OFDM-IM'in yukarıda bahsedilen avantajlarından yararlanılarak iki özgün OFDM-IM tabanlı çok taşıyıcılı iletim şeması önerilmiştir.

İlk olarak, bir alt bloktaki alt taşıyıcıların sayısına eşit bir çeşitlilik kazancı elde etmek için alt taşıyıcılarda koordinat serpiştirme ve güç dağıtımı uygulayan güç dağıtım IM'li koordinat serpiştirilmiş OFDM (coordinate interleaved OFDM with power distribution IM, CI-OFDM-PIM) olarak adlandırılan yeni bir iletim şeması önerilmiştir. CI-OFDM-PIM için ortalama bit hata olasılığı (average bit error rate, ABEP) türetilmiş ve önerilen şemanın referanslarına kıyasen sahip olduğu üstün hata performansı bilgisayar simülasyonları aracılığıyla gösterilmiştir.

Sonrasında ise iki olan çeşitlilik mertebesi ve akıllı alt taşıyıcı etkinleştirme paterni (subcarrier activation pattern, SAP) algılama mekanizması sayesinde üstün hata performansı ve gelişmiş bant verimliliği sağlayan, tekrarlanmış fazda/dik IM'li koordinat serpiştirilmiş OFDM (coordinate interleaved OFDM with repeated in phase/quadrature IM, CI-OFDM-RIQIM) adı verilen yeni bir OFDM-IM tabanlı şema önerilmiştir. Ayrıca, önerilen şema için bir logaritmik olasılık oranı (log-likelihood ratio, LLR) tabanlı düşük karmaşıklıkta alıcı tasarlanmıştır. Teorik analizler yapıldı ve bit hata olasılığı (bit error rate, BER) için bir üst sınır türetildi. Önerilen ve referans şemaları karşılaştırmak için tam ve eksik kanal durum bilgisi (channel state information, CSI) altında kapsamlı bilgisayar simülasyonları yürütüldü. CI-OFDM-RIQIM'in üstün sonuçlar gösterdiği ve yeni nesil kablosuz iletişim sistemleri için umut verici bir aday olarak kabul edilebileceği gösterilmiştir.

ACKNOWLEDGMENTS

First of all, I would like to express my deepest gratitude to my dear advisor, Assoc. Prof. Ertuğrul Başar for his faith in me and continuous support during my master degree process. I am grateful to him for guiding me in every aspect besides my academic studies.

Secondly, I would like to thank my lovely mother Fatma Tuğtekin, and dear father Hüseyin Tuğtekin, for bringing me to where I am today. Additionally, I feel very lucky to be the elder brother of my lovely siblings Yusuf Sefa, Betül, and Muhammed Fatih because of their kind respect and endless support for me. Besides, I am very grateful to my beloved Cansu for being my second family with her endless belief in me.

I would also like to thank dear Ali Tuğberk for his academic guidance, continuous support and precious friendship.

I am very grateful to be a member of the CoreLab family. I will forever remember the times we spent in front of the A2-Z02, the lahmacuns we ate and the football matches we played.

Last but not least, I would like to appreciate my dear high school friends and Chegg The Band brothers, who are my siblings from another mother, for always being there for me.

TABLE OF CONTENTS

LIST OF TABLES

LIST OF FIGURES

ABBREVIATIONS

ABEP	Average Bit Error Probability
AR	Augmented Reality
BER	Bit Error Rate
CIOD	Coordinate Interleaved Orthogonal Design
CIR	Channel Impulse Response
CM	Complex Multiplication
CP	Cyclic Prefix
CPEP	Conditional Pairwise Error Probability
CSI	Channel State Information
eMBB	Enhanced Mobile Broadband
FFT	Fast Fourier Transform
IEEE	Institute of Electrical and Electronics Engineers
IFFT	Inverse Fast Fourier Transform
IM	Index Modulation
LLR	Log-Likelihood Ratio
MAP	Mode Activation Pattern
MCGD	Minimum Coding Gain Distance
MDS	Maximum-Distance Separable
MIMO	Multiple-Input Multiple-Output
ML	Maximum Likelihood
mMTC	Massive Machine-Type Communications
NOMA	Non-Orthogonal Multiple Access

OFDM	Orthogonal Frequency Division Multiplexing
PEP	Pairwise Error Probability
PSK	Phase Shift Keying
QAM	Quadrature Amplitude Modulation
SAP	Subcarrier Activation Pattern
SNR	Signal-to-Noise Ratio
UPEP	Unconditional Pairwise Error Probability
URLLC	Ultra-Reliable and Low-Latency Communications
VR	Virtual Reality

Chapter 1

INTRODUCTION

Wireless communication systems have a very important place in our lives since both transmission and reception of data in a secured and wireless way is a must for today's technology. Accordingly, wireless technologies are widely used with many state-of-the-art systems in an incorporated manner. Nonetheless, next generation wireless communication standards require advanced features in order to meet the various needs of applications in future networks. For example, advanced reliability and higher data transmission rates are required by ultra-reliable low-latency communications (URLLC) and enhanced mobile broadband (eMBB), respectively. Furthermore, depending on the completely distinct needs of these networks and their specific usage areas in the practical life, more sophisticated waveforms should be designed. Since multicarrier transmission systems provide a robustness to both interference and fading, they are widely utilized in waveform designs.

Orthogonal frequency division multiplexing (OFDM) is one of the most commonly used multicarrier transmission schemes and has been included in several communication standards. Due to various advantages of OFDM such as robustness to inter-symbol interference, simplicity and suitability, it is still commonly used in the modern communication technologies. Moreover, a variety of studies have been proposed in the literature to improve the performance of OFDM. In [Sasamori et al., 2011], OFDM subcarriers are repetition coded to obtain a diversity gain, resulting in enhanced error performance. However, it is challenging to obtain higher spectral efficiencies with OFDM for frequency selective fading channels since information bits are transmitted only by M-ary signal constellations.

Index modulation (IM), in which indices of the building blocks such as transmit antennas and subcarriers, are utilized for the tranmission of the additional information bits, has attracted much attention in the literature [Basar, 2016]. Flexibility, low complexity, and high spectral efficiency of IM, make it a great candidate for the next generation communication systems. In OFDM with IM (OFDM-IM) [Başar et al., 2013], IM is well employed in the OFDM by transmitting additional information bits through the indices of the active subcarriers.

1.1 Contributions to the Literature

In this thesis, first, a novel scheme called *coordinate interleaved OFDM with power distribution IM (CI-OFDM-PIM)*, which provides an additional diversity gain over OFDM-IM, is proposed. In this scheme, data symbols are first rotated and coordinate interleaved, then distributed over two different subcarriers with high and low power levels. Due to its clever subcarrier activation pattern (SAP) selection strategy, coordinate interleaving, and power distribution, the proposed method can provide a diversity gain which is equal to the subblock size. Since power distribution method makes the repeated coordinate interleaved data symbols distinguishable by multiplying them with two different power levels, transmitting information bits by IM becomes possible. Moreover, the optimum power levels and rotation angles have been obtained to maximize the minimum coding gain distance (MCGD). Transceiver architecture for the proposed scheme is given and upper bound for the average bit error probability (ABEP) is derived. It is demonstrated via computer simulations that proposed scheme has better error performance than its benchmarks with a diversity order of two.

Secondly, a novel OFDM-IM based transmission scheme named *coordinate interleaved OFDM with repeated in-phase/quadrature IM (CI-OFDM-RIQIM)*, which provides additional diversity gain compared to conventional OFDM-IM, is proposed. In this scheme, all subblocks are first divided into two clusters with equal sizes. The real and imaginary parts from the first half of the data symbol vector are transmitted over the active subcarriers in the first and second clusters, respectively. Moreover, the real and imaginary parts of the second half of the data symbol vector are transmitted over the active subcarriers in the second and first clusters, respectively. Since the same SAPs are exploited to transmit the real and imaginary parts of data symbols, information bits conveyed by IM are more preserved. Since the real and imaginary parts of each data symbol are conveyed over two distinct subcarriers, a diversity order of two is guaranteed in the proposed scheme. In addition, a low-complexity log-likelihood ratio (LLR) based detector is provided for proposed scheme and an upper bound for the ABEP is derived. Furthermore, a diversity analysis is performed, and an optimum rotation angle selection strategy is presented. Error performance comparisons between the proposed and benchmark schemes are presented through comprehensive computer simulations under perfect and imperfect channel state information (CSI).

These aforementioned contributions are considered as two journal papers. CI-OFDM-PIM has been published in the *Institute of Electrical and Electronics Engineers (IEEE) Communication Letters*. CI-OFDM-RIQIM has been submitted to *IEEE Transactions on Wireless Communications*.

Notations: Bold, lowercase and capital letters stand for vectors and matrices, respectively. $(\cdot)^{\mathrm{H}}$, $(\cdot)^{\mathrm{T}}$, and $\mathrm{diag}(\cdot)$ are used for Hermitian, transposition, and diagonalization operations, respectively. $\mathbf{I}_{N\times N}$ refer to $N \times N$ identify matrix. The determinant and rank of a matrix is represented by $\det(\cdot)$ and $\mathrm{rank}(\cdot)$, respectively. $X \sim \mathcal{CN}(0, \sigma_X^2)$ denotes the distribution of a circularly symmetric complex Gaussian random variable X with variance σ_X^2. Binomial coefficient is represented by $\binom{n}{k}$. $\|\cdot\|$, $E\{\cdot\}$, and $\lfloor\cdot\rfloor$ are used for Euclidean norm, expectation, and floor function, respectively.

Chapter 2

ORTHOGONAL FREQUENCY DIVISION MULTIPLEXING WITH INDEX MODULATION

In this chapter, system model and a literature review for OFDM-IM are presented, respectively.

2.1 System Model of OFDM-IM

OFDM-IM is based on an OFDM transmission system with N number of subcarriers as seen in Fig. 2.1. A total number of m bits enter the transmitter and those are separated into G blocks, where each group includes $m/G = p = p_1 + p_2$ bits, to form a subblock with length $n = N/G$. For the creation of ζth subblock $\mathbf{x}_\zeta$, first $p_1 = \lfloor \log_2 \binom{n}{k} \rfloor$ bits determine the indices of the active subcarriers as:

$$\mathbf{i}_\zeta = [i_\zeta(1), \cdots, i_\zeta(k)], \tag{2.1}$$

where $i_\zeta(\alpha) \in \{1, 2, \cdots, n\}$, $\alpha = 1, \cdots, k$, and k is the number of active subcarriers. Secondly, modulated data symbols are determined by $p_2 = k \log_2(M)$ bits as:

$$\mathbf{s}_\zeta = [s_\zeta(1), \cdots, s_\zeta(k)],\ s_\zeta(\alpha) \in \mathcal{S} \tag{2.2}$$

where $\mathcal{S}$ is the M-ary signal constellation that is normalized to unity and M is the modulation order. Then, $\mathbf{x}_\zeta$ is created by considering $\mathbf{i}_\zeta$ and $\mathbf{s}_\zeta$. Finally, after applying the same steps to all subblocks and concatenating them, whole OFDM block is created as:

$$\begin{aligned}\mathbf{x} &= [\mathbf{x}_1^{\mathbf{T}} \mathbf{x}_2^{\mathbf{T}} \cdots \mathbf{x}_G^{\mathbf{T}}] \\ &= [x(1) \cdots x(N)].\end{aligned} \tag{2.3}$$

Subsequently, the time domain signal is obtained by taking inverse fast Fourier Transform (IFFT). After adding cyclic prefix (CP) with length L to the beginning of

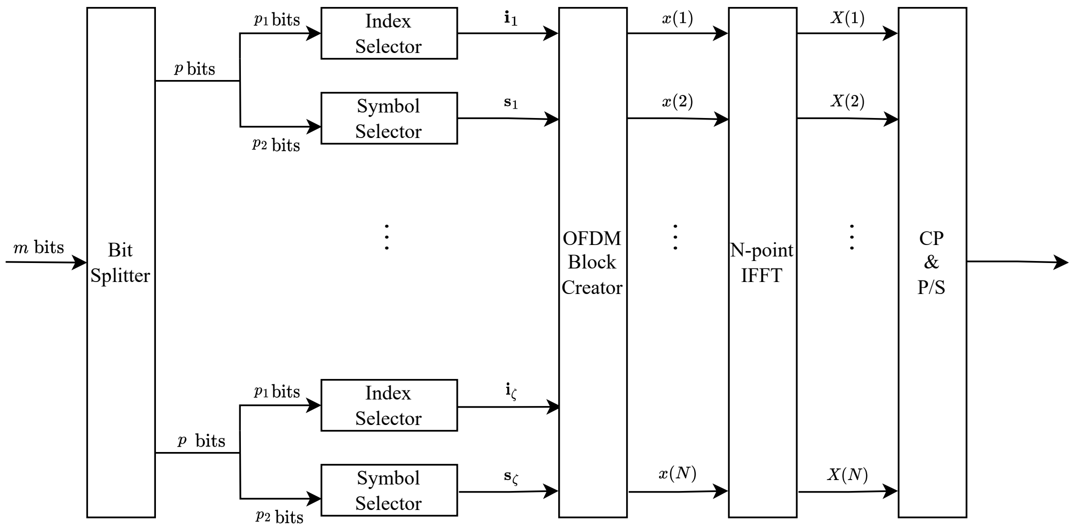

Figure 2.1: Block diagram of the OFDM-IM transmitter.

the OFDM frame and employing parallel to serial (P/S) and digital/analog transformation, the time-domain OFDM signal is transmitted through a T-tap frequency-selective Rayleigh fading channel whose elements follows circularly symmetric complex Gaussian random variables with the $\mathcal{CN}(0, 1/T)$. At the receiver side, after removing CP, FFT and deinterleaver are applied to obtain the frequency domain signal. Consequently, the equivalent input-output equation for the ζth subblock in the frequency domain can be indicated as:

$$\mathbf{y}_\zeta = \mathbf{X}_\zeta \mathbf{h}_\zeta + \mathbf{n}_\zeta, \tag{2.4}$$

where $\mathbf{X}_\zeta = \text{diag}(\mathbf{x}_\zeta)$, $\mathbf{y}_\zeta$, $\mathbf{h}_\zeta = [h_{\zeta,1}, \cdots, h_{\zeta,N}]^\mathrm{T}$, and $\mathbf{n}_g = [n_{g,1}, \cdots, n_{\zeta,N}]^\mathrm{T}$ are the transmitted signal, received signal vector, channel coefficients, and noise vector for the corresponding ζth subblock, respectively, where $h_\epsilon \sim \mathcal{CN}(0, 1)$, $n_\epsilon \sim \mathcal{CN}(0, N_0)$, $\epsilon = 1, \cdots, N$, and N_0 is the noise variance.

The maximum-likelihood (ML) detection can be employed to detect the ζ^{th} subblock by utilizing the set $\mathcal{X} = \{\mathbf{x}_1, \mathbf{x}_2, \cdots, \mathbf{x}_{2^p}\}$ which contains all possible subblock realizations:

$$\hat{\mathbf{x}}_\zeta = \arg\min_{\mathbf{x}_\zeta \in \mathcal{X}} \|\mathbf{y}_\zeta - \mathbf{X}_\zeta \mathbf{h}_\zeta\|^2. \tag{2.5}$$

Since information bits are more preserved against fading when they are transmitted by IM rather than classical M-ary PSK/QAM modulation, OFDM-IM shows superior error performance over the conventional OFDM. Moreover, OFDM-IM attracts much attention in the literature due to its several advantages such as high flexibility and implementation simplicity.

2.2 A Literature Review on OFDM-IM

OFDM-IM is a promising multicarrier transmission scheme and has attracted the attention of researchers due to numerous benefits such as flexibility and simplicity. To further enhance the flexibility, OFDM with generalized IM (OFDM-GIM), in which the number of active subcarriers in a subblock is no longer fixed, is proposed in [Fan et al., 2014]. In addition, the spectral efficiency of OFDM-IM has been improved by OFDM with in-phase/quadrature IM (OFDM-IQ-IM) [Zheng et al., 2015] where IM is performed on in-phase and quadrature components independently, doubling the number of IM bits. Moreover, OFDM with subcarrier number modulation (OFDM-SNM) is proposed in [Jaradat et al., 2018], where the number of the active subcarriers in a subblock is determined by incoming data bits, resulting in an enhanced spectral efficiency. Additionally, a block interleaver is employed in the subcarrier-level in [Xiao et al., 2014] to improve the error performance of OFDM-IM. Furthermore, many schemes have been proposed to address the diverse requirements of 5G services such as improved reliability, higher spectral and energy efficiency, and low complexity, by utilizing the flexibility of IM. For example, OFDM with hybrid number and IM (OFDM-HNIM) [Jaradat et al., 2020] and sparse-encoded codebook IM (SE-CBIM) [Arslan et al., 2020] are introduced to meet the requirements of different 5G services such as massive machine type communications (mMTC) and ultra-reliable low-latency communications (URLLC), respectively. Due to its simple and flexible structure, OFDM-IM can be combined with several emerging wireless communication systems such as multiple-input multiple-output (MIMO) [Basar, 2016, Lu et al., 2018, Chen and Zheng, 2018, Wang, 2021], non-orthogonal multiple access (NOMA) [Tusha et al., 2020, Chen et al., 2020, Doğan et al., 2019, Arslan et al., 2020, Şahin and Arslan, 2020], joint radar communication [Sahin et al., 2021], and optical communication systems [Azim et al., 2020, Başar and Panayırcı, 2015].

2.2.1 OFDM-IM Based Multiple-mode Schemes

Due to its de-activated subcarriers, it is challenging for OFDM-IM to provide high spectral efficiency. With this purpose, dual-mode aided OFDM (DM-OFDM) is proposed in [Mao et al., 2016], where null subcarriers are modulated by a secondary distinguishable constellation to transmit data symbols. The authors in [Mao et al., 2016], extend the work in [Mao et al., 2016] to a generalized form by varying the number of subcarriers modulated by the same mode. To further increase the number of bits transmitted by IM, multiple-mode OFDM-IM (MM-OFDM-IM), which exploits multiple signal constellations and their full permutations to perform IM, is proposed in [Wen et al., 2017]. MM-OFDM-IM is generalized in [Wen et al., 2018], where the size of the constellations can be different from each other while the number of bits transmitted via IM remains unchanged. $\mathcal{Q}$-ary MM-OFDM-IM ($\mathcal{Q}$-MM-OFDM-IM) is proposed in [Yarkin and Coon, 2020], where each subcarrier is modulated by $\mathcal{Q}$ disjoint M-ary constellations repeatedly and a maximum-distance separable (MDS) code is utilized in the indices of these constellations, resulting in a higher number of index symbols. Furthermore, OFDM implementations with MDS amplitude and phase modulation (MDS-APM) and MDS in-phase and quadrature modulation (MDS-IQM) are given in [Yarkin and Coon, 2022]. Super-mode OFDM-IM (SuM-OFDM-IM) [Dogukan and Basar, 2020], which jointly determines mode activation patterns (MAPs) and subcarrier activation patterns (SAPs) is proposed to further increase the number of information bits transmitted by IM. OFDM with set partition modulation (OFDM-SPM), which differentiates subsets in a set partition by distinguishable constellations to achieve better error performance, is proposed in [Yarkin and Coon, 2020]. In addition, OFDM with transmit diversity (OFDM-TD), where null subcarriers are activated to convey the same information with active subcarriers by utilizing multiple constellations, is proposed in [Zheng and Chen, 2017]. Since all subcarriers are activated, these schemes can achieve higher spectral efficiency values compared to OFDM-IM. Therefore, they can be considered as candidate schemes for future enhanced mobile broadband (eMBB) services such as augmented/virtual reality (AR/VR).

2.2.2 Diversity Achieving OFDM-IM Based Schemes

To combat multi-path fading in wireless communication systems and provide better reliability, numerous OFDM-IM-based schemes, which yield additional diversity gain, are proposed in the literature. Repeated IM-OFDM (ReMO), which transmits the same data symbol over the activated subcarriers to achieve a transmit diversity, is proposed in [Van Luong et al., 2018]. Moreover, coded OFDM-IM is incorporated with a simple transmit diversity scheme to enhance the error performance of OFDM-IM [Choi, 2017]. Coordinate interleaved OFDM-IM (CI-OFDM-IM) [Başar, 2015] transmits the real and imaginary parts of the data symbols over different subcarriers and provides a diversity order of two. Another novel scheme called OFDM with power distribution IM (OFDM-PIM) that provides additional diversity gain by conveying data symbols through two subcarriers with high and low power levels, is introduced in [Dogukan and Basar, 2020]. In [Thanh et al., 2018], repeated IM-OFDM with CI (RIM-OFDM-CI) is proposed, where data symbols from different clusters are coordinate interleaved. Furthermore, the same indices of subcarriers in both clusters are exploited to transmit the coordinate interleaved data symbols resulting in improved detection of index bits. It has been demonstrated that RIM-OFDM-CI provides a better error performance than OFDM-IM and CI-OFDM-IM at the same spectral efficiency. In [Le et al., 2021], the authors extend their work in [Thanh et al., 2018] by optimizing the rotation angle for the signal constellation with detailed theoretical analysis and developing low-complexity detectors to reduce receiver complexity. A comparison for the aforementioned OFDM-IM based schemes in terms of the ML detection complexity, BER performance, and spectral efficiency, is given in the Table 2.1. Furthermore, a comprehensive survey about OFDM-IM-based schemes is presented in [Mao et al., 2018].

Table 2.1: Comparison of the OFDM-IM Based Schemes in terms of the ML Detection Complexity, BER Performance, and Spectral Efficiency

System	ML Detection Complexity	BER Performance	Spectral Efficiency
OFDM-IM	Medium	Low	Low
OFDM-GIM	Medium	Medium	Low
OFDM-IQ-IM	Medium	Medium	Medium
OFDM-SNM	Medium	Low	Medium
OFDM-HNIM	Medium	Low	Low
DM-OFDM	High	Medium	High
MM-OFDM-IM	High	Medium	High
SuM-OFDM-IM	High	High	High
ReMO	High	High	Low
CI-OFDM-IM	High	High	Low
OFDM-PIM	High	High	Medium
RIM-OFDM-CI	High	High	Low

Chapter 3

COORDINATE INTERLEAVED OFDM WITH POWER DISTRIBUTION INDEX MODULATION

Despite the remarkable improvements in the literature, there is still an obvious necessity for OFDM-IM-based waveform designs that can provide superior error performance to provide needs of future wireless communication services such as eMBB applications.

CI-OFDM-PIM is a novel OFDM-IM based transmission scheme which provides a diversity gain that is equal to the subblock size due to its clever SAP selection strategy, coordinate interleaving, and power distribution. Thus, since CI-OFDM-PIM can provide a higher diversity order compared to the OFDM-IM based schemes, it shows a superior BER performance.

In this chapter, the system model, performance analysis including optimization, and simulations results of CI-OFDM-PIM are given, respectively.

3.1 System Model of CI-OFDM-PIM

CI-OFDM-PIM is based on an OFDM transmission system with S number of subcarriers as seen in Fig. 3.1. A total number of m bits enter the transmitter and those are separated into G blocks, where each group includes $m/G = p = p_1 + p_2$ bits, to form a subblock with length $N = S/G$, where N is an even number and greater than 2. Since the same process is applied to all subblocks, we present the creation of gth subblock $\mathbf{c}_g$, $g = [1, \cdots, G]$. For the sake of simplicity, we remove the subscript g. The block diagram for the generation of the gth subblock is given in Fig. 3.2. Firstly, $p_1 = (N/2)\log_2(M)$ bits determine the $N/2$ data symbols $\mathbf{x} = [x_1, \cdots, x_{N/2}]^{\mathrm{T}} \in \mathbb{C}^{N/2}$, where M is the modulation order. Constellation rotation, which is a must to obtain a diversity gain and increase the cod-

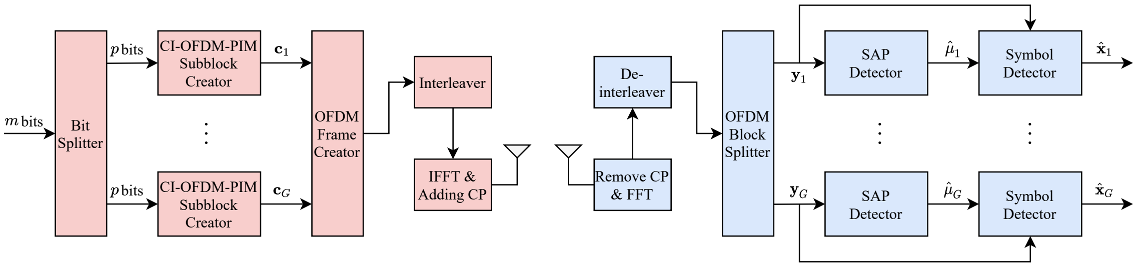

Figure 3.1: Transceiver architecture of CI-OFDM-PIM including single-symbol ML detector.

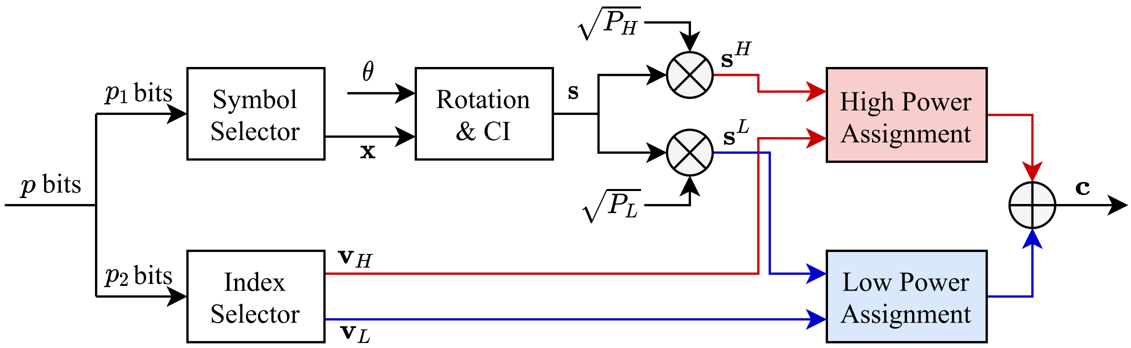

Figure 3.2: The block diagram of the creation of the gth subblock of CI-OFDM-PIM.

ing gain, is a significant component of a coordinate interleaving-based transmission schemes [Khan and Rajan, 2006]. The nth element of $\mathbf{x}$ is rotated with an angle θ_n, $n = 1, 2, \cdots, N/2$, and the rotated data symbol vector is obtained as:

$$\begin{aligned}\mathbf{x}^{\theta} &= [x_1 e^{j\theta_1}, x_2 e^{j\theta_2}, \cdots, x_{N/2} e^{j\theta_{N/2}}]^{\mathrm{T}} \\ &= [\bar{x}_1, \bar{x}_2, \cdots, \bar{x}_{N/2}]^{\mathrm{T}}.\end{aligned} \tag{3.1}$$

After this, CI is applied to $\mathbf{x}^{\theta}$ and coordinate interleaved data symbol vector is obtained as:

$$\mathbf{s} = \begin{bmatrix} s_1 \\ s_2 \\ \vdots \\ s_{N/2-1} \\ s_{N/2} \end{bmatrix} = \begin{bmatrix} \bar{x}_1^R + j\bar{x}_2^I \\ \bar{x}_2^R + j\bar{x}_1^I \\ \vdots \\ \bar{x}_{N/2-1}^R + j\bar{x}_{N/2}^I \\ \bar{x}_{N/2}^R + j\bar{x}_{N/2-1}^I \end{bmatrix}. \tag{3.2}$$

Here, two power levels are specified as P_H (high) and P_L (low) for the subcarriers with high and low power, respectively, where $P_H > P_L$ and $P_H + P_L = 2$ since the average power of a subcarrier is normalized to unity, i.e., $E\{\mathbf{c}^{\mathrm{H}}\mathbf{c}\} = N$. Then, $p_2 = \log_2(N)$ bits determine the SAP $\mathbf{v} = [v_1, v_2, \cdots, v_N]^{\mathrm{T}}$, $v_\chi \in \{1, \cdots, N\}$, $\chi = 1, 2, \cdots, N$. Note that the method for creating SAPs and the reason for using only N SAPs to convey bits are given as a remark in the following. The first half and second half of $\mathbf{v}$ represent the indices of subcarriers with high power and low power as $\mathbf{v}_H = [v_1, \cdots, v_{N/2}]^{\mathrm{T}}$ and $\mathbf{v}_L = [v_{N/2+1}, \cdots, v_N]^{\mathrm{T}}$, respectively. As a result, a total number of $p = p_1 + p_2 = (N/2)\log_2(M) + \log_2(N)$ bits can be conveyed for each subblock. After that, the coordinate interleaved data symbol vector is multiplied with $\sqrt{P_H}$ and $\sqrt{P_L}$, then high and low power data symbol vectors are obtained as $\mathbf{s}^H = \sqrt{P_H}\mathbf{s}$ and $\mathbf{s}^L = \sqrt{P_L}\mathbf{s}$, respectively. Finally, the entries of $\mathbf{s}^H$ and $\mathbf{s}^L$ are placed into the target subblock $\mathbf{c}$ with the entries of $\mathbf{v}_H$ and $\mathbf{v}_L$, respectively. The selection strategy of P_H, P_L, and $\boldsymbol{\theta} = [\theta_1, \cdots, \theta_{N/2}]^{\mathrm{T}}$ is discussed in the Section III.

Remark (SAP Creation): The minimum distance of a set $\mathcal{Z}$ of codewords with length N_c is defined as $d = \min_{z_1, z_2 \in \mathcal{Z}, z_1 \neq z_2} d(z_1, z_2)$, where $d(z_1, z_2)$ represents the Hamming distance between z_1 and z_2. In a Q-ary block code of length N_c and minimum distance d, the number $A_Q(N_c, d)$ indicates the maximum number of possible codewords. Here, Singleton bound states that $A_Q(N_c, d) \leq Q^{N_c - d + 1}$ [Singleton, 1964]. In the proposed method, all possible SAPs can be considered as codewords in a N-ary block code of length N. To provide a diversity order of N, d should be selected as N; hence, a total $Q^{N_c - d + 1} = N^{N - N + 1} = N$ number of SAPs can be utilized for the transmission of index bits according to the Singleton bound. There are a total number of $2^{p_2} = N$ possible SAPs. The first SAP is given as $(\mathbf{v})_1 = [1, 2, \cdots, N]^{\mathbf{T}}$ and μth SAP $(\mathbf{v})_\mu$ can be obtained by circularly shifting $(\mathbf{v})_1$ with $\mu - 1$ elements.

For simplicity, we provide an example below for the creation of a subblock. *Example:* Assume that $N = 4$, $p_2 = [0\,0]$, $\mathbf{s} = [s_1\, s_2]^{\mathrm{T}}$, and all possible SAPs can be obtained as in Table 3.1. There are $N = 4$ possible $\mathbf{v} = [\mathbf{v}_H^{\mathrm{T}} \mathbf{v}_L^{\mathrm{T}}]^{\mathrm{T}}$ vectors and the Hamming distance between each $\mathbf{v}$ pair is $N = 4$. According to incoming $p_2 = [0\,0]$ bits, $\mathbf{v}_H = [1, 2]^{\mathrm{T}}$ and $\mathbf{v}_L = [3, 4]^{\mathrm{T}}$. With these parameters, the example subblock is

Table 3.1: The subcarrier indices according to incoming p_2 bits for $N = 4$.

p_2 bits	$\mathbf{v}_H^{\mathrm{T}}$	$\mathbf{v}_L^{\mathrm{T}}$	$\mathbf{c}^{\mathrm{T}}$
[00]	$[1,2]$	$[3,4]$	$[s_1^H s_2^H s_1^L s_2^L]$
[01]	$[4,1]$	$[2,3]$	$[s_2^H s_1^L s_2^L s_1^H]$
[10]	$[3,4]$	$[1,2]$	$[s_1^L s_2^L s_1^H s_2^H]$
[11]	$[2,3]$	$[4,1]$	$[s_2^L s_1^H s_2^H s_1^L]$

created as:

$$\mathbf{c} = [s_1^H, s_2^H, s_1^L, s_2^L]^{\mathrm{T}}, \tag{3.3}$$

where $s_a^H = \sqrt{P_H} s_a$ and $s_a^L = \sqrt{P_L} s_a$ represent the coordinate interleaved data symbols with high and low power, respectively, and $a = 1, 2$.

By following the same steps for all subblocks, the whole OFDM frame is generated. Then, a block-type interleaver is applied as in [Başar, 2015]. After taking inverse fast Fourier transform (IFFT) and inserting cyclic prefix (CP) with length S_{CP}, the time-domain signal is obtained and transmitted over T-tap frequency selective Rayleigh fading channel whose elements follow $\mathcal{CN}(0, 1/T)$ distribution. At the receiver side, after removing CP, FFT and deinterleaver are applied to obtain the frequency domain signal. The equivalent input-output equation for the gth subblock in the frequency domain can be indicated as:

$$\mathbf{y}_g = \mathbf{C}_g \mathbf{h}_g + \mathbf{w}_g, \tag{3.4}$$

where $\mathbf{y}_g$, $\mathbf{h}_g = [h_{g,1}, \cdots, h_{g,N}]^{\mathrm{T}}$, and $\mathbf{w}_g = [w_{g,1}, \cdots, w_{g,N}]^{\mathrm{T}}$ are the received signal vector, channel coefficients, and noise vector for the corresponding gth subblock, respectively, where $h_\epsilon \sim \mathcal{CN}(0, 1)$, $w_\epsilon \sim \mathcal{CN}(0, N_0)$, $\epsilon = 1, \cdots, N$, and $\mathbf{C}_g = \mathrm{diag}(\mathbf{c}_g)$. We define the signal-to-noise (SNR) ratio as $\Gamma = E_b/N_0$, where $E_b = (S + S_{\mathrm{CP}})/m$ is the average bit energy. In order to detect the gth subblock, the maximum-likelihood (ML) rule can be applied by employing the set $\{\mathbf{c}_1, \mathbf{c}_2, \cdots, \mathbf{c}_{2^p}\} \in \mathcal{C}$ which consists of all possible subblock realizations:

$$\hat{\mathbf{c}}_g = \arg\min_{\mathbf{c}_g \in \mathcal{C}} \|\mathbf{y}_g - \mathbf{C}_g \mathbf{h}_g\|^2. \tag{3.5}$$

The number of metrics calculated in (3.5) is $NM^{N/2}$ and therefore, the ML detector becomes significantly complicated for high values of N and M. The number of metrics calculated for detection can be reduced by exploiting single-symbol ML decoding property of coordinate interleaved orthogonal designs (CIODs) as in [Başar, 2015]. For the gth subblock, (3.4) may be rewritten without losing generality as follows:

$$\begin{bmatrix} y_1 \\ \vdots \\ y_N \end{bmatrix} = \begin{bmatrix} c_1 & & \\ & \ddots & \\ & & c_N \end{bmatrix} \begin{bmatrix} h_1 \\ \vdots \\ h_N \end{bmatrix} + \begin{bmatrix} w_1 \\ \vdots \\ w_N \end{bmatrix}. \tag{3.6}$$

For each realization of $(\mathbf{v})_\mu = ([\mathbf{v}_H^{\mathrm{T}} \mathbf{v}_L^{\mathrm{T}}]^{\mathrm{T}})_\mu$, $\mu = 1, \cdots, N$, N equivalent channel models can be obtained for each pair of $(\mathbf{x}_\alpha, \mathbf{x}_\beta)$ by the ML detector as:

$$\begin{bmatrix} y^R_{v_{2\alpha-1}} \\ y^I_{v_{2\alpha-1}} \\ y^R_{v_{2\alpha}} \\ y^I_{v_{2\alpha}} \\ y^R_{v_{2\beta-1}} \\ y^I_{v_{2\beta-1}} \\ y^R_{v_{2\beta}} \\ y^I_{v_{2\beta}} \end{bmatrix}_\mu = \begin{bmatrix} h^R_{v_{2\alpha-1}} & 0 & 0 & 0 & 0 & -h^I_{v_{2\alpha-1}} & 0 & 0 \\ h^I_{v_{2\alpha-1}} & 0 & 0 & 0 & 0 & h^R_{v_{2\alpha-1}} & 0 & 0 \\ 0 & -h^I_{v_{2\alpha}} & 0 & 0 & h^R_{v_{2\alpha}} & 0 & 0 & 0 \\ 0 & h^R_{v_{2\alpha}} & 0 & 0 & h^I_{v_{2\alpha}} & 0 & 0 & 0 \\ 0 & 0 & h^R_{v_{2\beta-1}} & 0 & 0 & 0 & 0 & -h^I_{v_{2\beta-1}} \\ 0 & 0 & h^I_{v_{2\beta-1}} & 0 & 0 & 0 & 0 & h^R_{v_{2\beta-1}} \\ 0 & 0 & 0 & -h^I_{v_{2\beta}} & 0 & 0 & h^R_{v_{2\beta}} & 0 \\ 0 & 0 & 0 & h^R_{v_{2\beta}} & 0 & 0 & h^I_{v_{2\beta}} & 0 \end{bmatrix}_\mu \times \begin{bmatrix} x_\alpha^{(H,R)} \\ x_\alpha^{(H,I)} \\ x_\alpha^{(L,R)} \\ x_\alpha^{(L,I)} \\ x_\beta^{(H,R)} \\ x_\beta^{(H,I)} \\ x_\beta^{(L,R)} \\ x_\beta^{(L,I)} \end{bmatrix} + \begin{bmatrix} w^R_{v_{2\alpha-1}} \\ w^I_{v_{2\alpha-1}} \\ w^R_{v_{2\alpha}} \\ w^I_{v_{2\alpha}} \\ w^R_{v_{2\beta-1}} \\ w^I_{v_{2\beta-1}} \\ w^R_{v_{2\beta}} \\ w^I_{v_{2\beta}} \end{bmatrix}_\mu, \tag{3.7}$$

where $\mathbf{x}_\gamma = [x_\gamma^H \; x_\gamma^L]^{\mathrm{T}}$, $\gamma \in \{\alpha, \beta\}$. We can rewrite (3.7) as:

$$\begin{aligned} (\tilde{\mathbf{y}}_\xi)_\mu =& (\tilde{\mathbf{H}}_\xi)_\mu \tilde{\mathbf{x}}_\xi + (\tilde{\mathbf{w}}_\xi)_\mu \\ =& [(\tilde{\mathbf{H}}_{\xi,1})_\mu \; (\tilde{\mathbf{H}}_{\xi,2})_\mu] \tilde{\mathbf{x}}_\xi + (\tilde{\mathbf{w}}_\xi)_\mu, \end{aligned} \tag{3.8}$$

where $\xi = 1, 2, \cdots, N/4$, $\alpha = 2\xi - 1$ and $\beta = 2\xi$. Since the columns of $(\tilde{\mathbf{H}}_\xi)_\mu$ are orthogonal, single symbol ML decoding can be applied and for each $(\mathbf{v})_\mu$ realization, the ML decoder computes the following metrics as:

$$\Delta(\mu) = \sum_{\xi=1}^{N/4} \Big(\min_{x_\alpha} \|(\tilde{\mathbf{y}}_\xi)_\mu - (\tilde{\mathbf{H}}_{\xi,1})_\mu \tilde{\mathbf{x}}_\alpha\|^2 + \min_{x_\beta} \|(\tilde{\mathbf{y}}_\xi)_\mu - (\tilde{\mathbf{H}}_{\xi,2})_\mu \tilde{\mathbf{x}}_\beta\|^2 \Big), \tag{3.9}$$

where $\tilde{\mathbf{x}}_\gamma = [x_\gamma^{(H,R)} x_\gamma^{(H,I)} x_\gamma^{(L,R)} x_\gamma^{(L,I)}]^{\mathrm{T}}$. Here, firstly, activated SAP $(\mathbf{v})_{\hat{\mu}}$ is determined by using $\hat{\mu} = \arg\min_{\mu} \Delta(\mu)$. Then, data symbols are decoded by using the following rules:

$$\begin{aligned} \hat{x}_\alpha &= \min_{x_\alpha} \|(\tilde{\mathbf{y}}_\xi)_{\hat{\mu}} - (\tilde{\mathbf{H}}_{\xi,1})_{\hat{\mu}} \tilde{\mathbf{x}}_\alpha\|^2 \\ \hat{x}_\beta &= \min_{x_\beta} \|(\tilde{\mathbf{y}}_\xi)_{\hat{\mu}} - (\tilde{\mathbf{H}}_{\xi,2})_{\hat{\mu}} \tilde{\mathbf{x}}_\beta\|^2. \end{aligned} \tag{3.10}$$

The same process is performed to detect SAPs, $(\mathbf{v})_{\hat{\mu}_1}, \cdots, (\mathbf{v})_{\hat{\mu}_G}$, and data symbols, $\hat{\mathbf{x}}_1, \cdots, \hat{\mathbf{x}}_G$, of all subblocks, $\hat{\mathbf{x}} = [\hat{x}_1, \cdots, \hat{x}_{N/2}]^{\mathrm{T}}$. Thanks to single-symbol ML detection, the number of metrics calculated for decoding decreases from $NM^{N/2}$ to $(N/2)NM$.

3.2 Performance Analysis and Optimization

In this section, we obtain an upper bound on the BER of CI-OFDM-PIM system under the assumption of ML detection. As in [Başar et al., 2013], ABEP of CI-OFDM-PIM can be obtained as:

$$P_b = \frac{1}{p2^p} \sum_{\mathbf{C},\hat{\mathbf{C}}} \mathrm{P}(\mathbf{C} \to \hat{\mathbf{C}}) \mathrm{e}(\mathbf{C}, \hat{\mathbf{C}}), \tag{3.11}$$

where $\mathrm{e}(\mathbf{C}, \hat{\mathbf{C}})$ is the number of erroneous bits when $\mathbf{C}$ is transmitted; however, $\hat{\mathbf{C}}$ is incorrectly detected and $\mathrm{P}(\mathbf{C} \to \hat{\mathbf{C}})$ is the pairwise error event for the corresponding pairwise event and given by

$$\mathrm{P}(\mathbf{C} \to \hat{\mathbf{C}}) \approx \frac{1/4}{\det(\mathbf{I}_N + (\Gamma/3)\mathbf{D})} + \frac{1/12}{\det(\mathbf{I}_N + (\Gamma/4)\mathbf{D})}, \tag{3.12}$$

where $\mathbf{D} = (\mathbf{C} - \hat{\mathbf{C}})^{\mathrm{H}} (\mathbf{C} - \hat{\mathbf{C}})$ is the $N \times N$ difference matrix.

In order to investigate the diversity order of CI-OFDM-PIM, two cases are considered: (1) detecting index bits erroneously and (2) detecting single or multiple data symbols under the condition of detecting index bits correctly. For case (1),

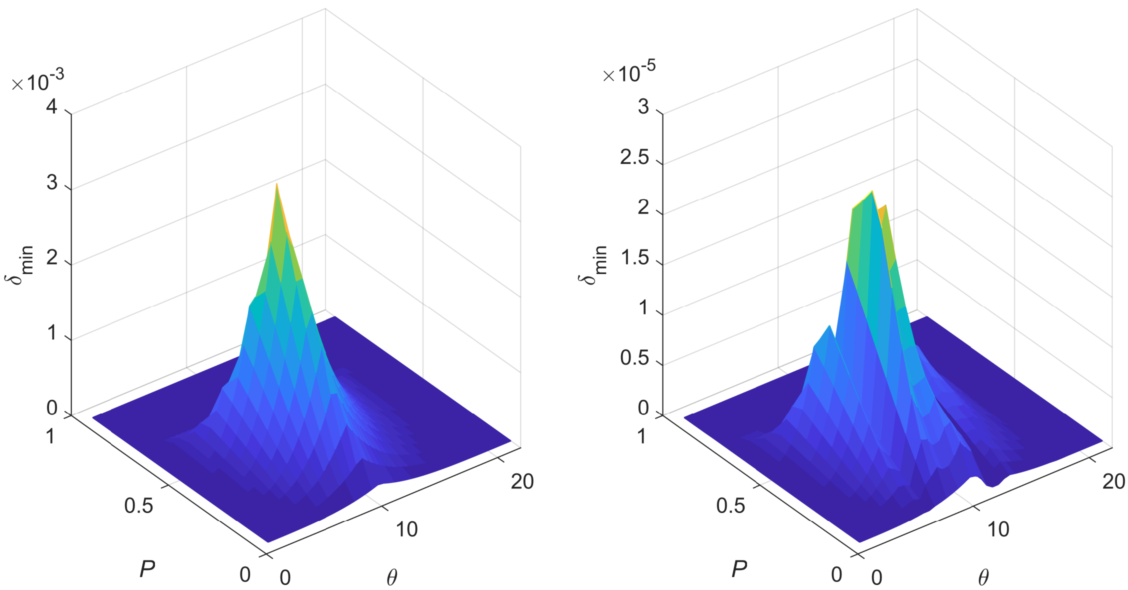

Figure 3.3: MCGD variation with respect to P and θ for 4-QAM and 8-QAM constellations, respectively.

assume that $p_2 = [00]$, $\mathbf{v} = [1, 2, 3, 4]^{\mathrm{T}}$, bits are transmitted; nonetheless, [01] bits, $\hat{\mathbf{v}} = [4, 1, 2, 3]^{\mathrm{T}}$, are decoded incorrectly from Table 3.1. As seen from this example, the Hamming distance between $\mathbf{v}$ and $\hat{\mathbf{v}}$ is $N = 4$. This result is valid for all other pairwise $(\mathbf{v}, \hat{\mathbf{v}})$ events and it can be concluded that the diversity order is always 4 for case (1). For case (2), assume that $\mathbf{c}$ with data symbols $(\bar{x}_1, \bar{x}_2)$, is transmitted, and $\hat{\mathbf{c}}$ with $(\bar{x}_1, \hat{\bar{x}}_2)$, is decoded erroneously with a single symbol error $(\bar{x}_2 \rightarrow \hat{\bar{x}}_2)$. This pair $(\mathbf{c}, \hat{\mathbf{c}})$ is given as:

$$
\begin{aligned}
\mathbf{c} &= [(\bar{x}_1^R + j\bar{x}_2^I)^H, (\bar{x}_2^R + j\bar{x}_1^I)^H, (\bar{x}_1^R + j\bar{x}_2^I)^L, (\bar{x}_2^R + j\bar{x}_1^I)^L]^{\mathrm{T}} \\
\hat{\mathbf{c}} &= [(\bar{x}_1^R + j\hat{\bar{x}}_2^I)^H, (\hat{\bar{x}}_2^R + j\bar{x}_1^I)^H, (\bar{x}_1^R + j\hat{\bar{x}}_2^I)^L, (\hat{\bar{x}}_2^R + j\bar{x}_1^I)^L]^{\mathrm{T}}.
\end{aligned} \tag{3.13}
$$

As seen from (3.13), only one symbol error causes changes over all subcarriers that resulting a diversity order of $r = N = 4$, where $r = \mathrm{rank}(\mathbf{D})$. Consequently, when non-zero and different rotation angles $[\theta_1, \cdots, \theta_{N/2}]$ are selected, we provide $\min_{\mathbf{C},\hat{\mathbf{C}}}(r) = 4$ which demonstrates that the diversity order of the proposed system is 4. By induction, the extension of cases (1) and (2) is valid for any value of N; hence, a diversity order of N is always provided.

The rotation angles $\boldsymbol{\theta}$ and power levels (P_H, P_L) affect the non-zero eigenvalues of $\mathbf{D}$ being λ_ζ, $\zeta = 1, 2, \cdots, N$, and as a consequence the ABEP. For simplicity, we define a single power level P, $0 < P < 1$, and rotation angle θ, where $P_H = 2 - P$, $P_L = P$, and θ_n is calculated with respect to θ as discussed in the sequel for $n = 1, \cdots, N/2$. We consider the worst case pairwise error probability (PEP) events to obtain the optimum θ and P values as:

$$(\theta_{\text{opt}}, P_{\text{opt}}) = \arg\max_{\theta,P} \delta_{\min}. \tag{3.14}$$

Here, $\delta_{\min} = \min_{\mathbf{C},\hat{\mathbf{C}}} \prod_{\zeta=1}^{N} \lambda_\zeta$ is the MCGD, which is a significant parameter for the minimization of (3.12). Due to a joint search over all possible P and θ_n values is not practically feasible, we propose a heuristic and near-optimal solution to find θ_{opt} and P_{opt} as follows. Since quadrature amplitude modulation (QAM) constellation repeats itself every 90°, we divide 90° into $N/2$ parts. In this case, we define the nth rotation angle as $\theta_n = \theta + 180(n-1)/N$, $0 < \theta < 90/N$, $n = 1, \cdots, N/2$. For example, as seen from Fig. 3.3, $(\theta_{\text{opt}}, P_{\text{opt}})$ can be obtained by exhaustive search as $(8.5°, 0.45)$ and $(8°, 0.40)$ for 4-QAM and 8-QAM, respectively, when $N = 4$. Here, the step sizes for $(\theta_{\text{opt}}, P_{\text{opt}})$ are $(0.5, 0.05)$. For higher values of M and N, carrying out an exhaustive search over all possible $(\mathbf{C}, \hat{\mathbf{C}})$ pairs is not practical. In this case, δ_{min} is evaluated for $\mathbf{C} \in \{\mathbf{C}^1\}$ and $\hat{\mathbf{C}} \in \{\mathbf{C}^1, \mathbf{C}^2\}$, where $\mathbf{C}^1 = \text{diag}([s_1^H, s_2^H, s_1^L, s_2^L]^{\text{T}})$ and $\mathbf{C}^2 = \text{diag}([s_1^L, s_2^L, s_1^H, s_2^H]^{\text{T}})$ are baseline worst case error events for $N = 4$. Here, two PEP events are considered: *i*) $(\mathbf{C}^1 \to \mathbf{C}^1)$: correct SAP with single erroneous data symbol, *ii*) $(\mathbf{C}^1 \to \mathbf{C}^2)$: detecting SAP as $N/2$ circularly shifted version of it with correct or erroneous data symbols.

3.3 Simulation Results and Comparisons

In this section, simulation results are demonstrated to compare CI-OFDM-PIM with benchmark schemes, given that the system parameters are $S = 128$, $S_{CP} = 16$ and $T = 10$ tap Rayleigh fading channel whose elements are independent identically distributed (i.i.d.) complex Gaussian distributed random variables. For convenience, we will refer to "OFDM-IM (N, v)" as OFDM-IM scheme with v out of N subcarriers are active, "DM-OFDM (N, v)" as DM-OFDM scheme where v out of N subcarriers exploits the primary M-ary PSK(or QAM) constellations, "SuM-OFDM-IM (M,

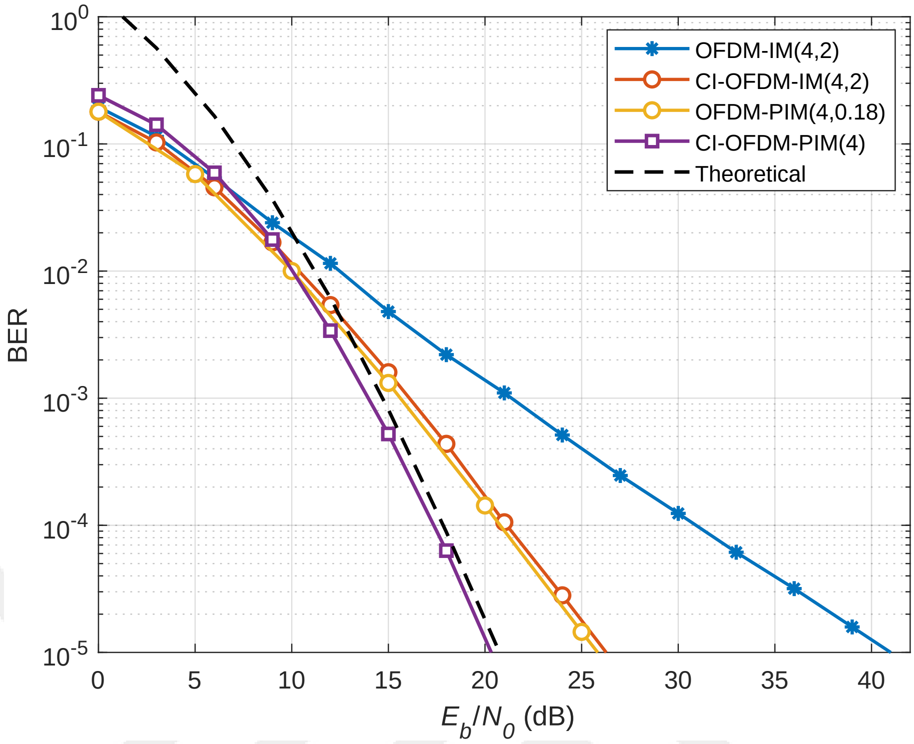

Figure 3.4: Error performance comparison of CI-OFDM-PIM with benchmark schemes when $N = 4$ and $M = 4$ for a spectral efficiency of 1.5 bps/Hz.

Q)" as SuM-OFDM-IM scheme with Q symbols included in each M mode, "CI-OFDM-IM (N, v)" as CI-OFDM-IM scheme with v out of N subcarriers are active, "OFDM-PIM $(N,\ P)$" as OFDM-PIM scheme with N subcarriers and optimum power of P , "RC-OFDM (n)" as RC-OFDM scheme with a repetition rate of n and "CI-OFDM-PIM (N)" is the proposed CI-OFDM-PIM scheme with N subblock length. Optimum angle and power level for the CI-OFDM-PIM is determined based on the selection strategy discussed in the Section III.

As seen in the Fig. 3.4, theoretical BER curve, which is obtained by (3.11), acts as an upper bound for CI-OFDM-PIM. Furthermore, CI-OFDM-PIM provides approximately 6 dB gain over CI-OFDM-IM and OFDM-PIM due to its higher diversity gain at a BER value of 10^{-5} when $N = 4$, $M = 4$, and the spectral efficiency is 1.5 bps/Hz.

In Fig. 3.5, the error performance of CI-OFDM-PIM is compared with classical OFDM, OFDM-IM, DM-OFDM, SuM-OFDM-IM, CI-OFDM-IM, OFDM-PIM, and

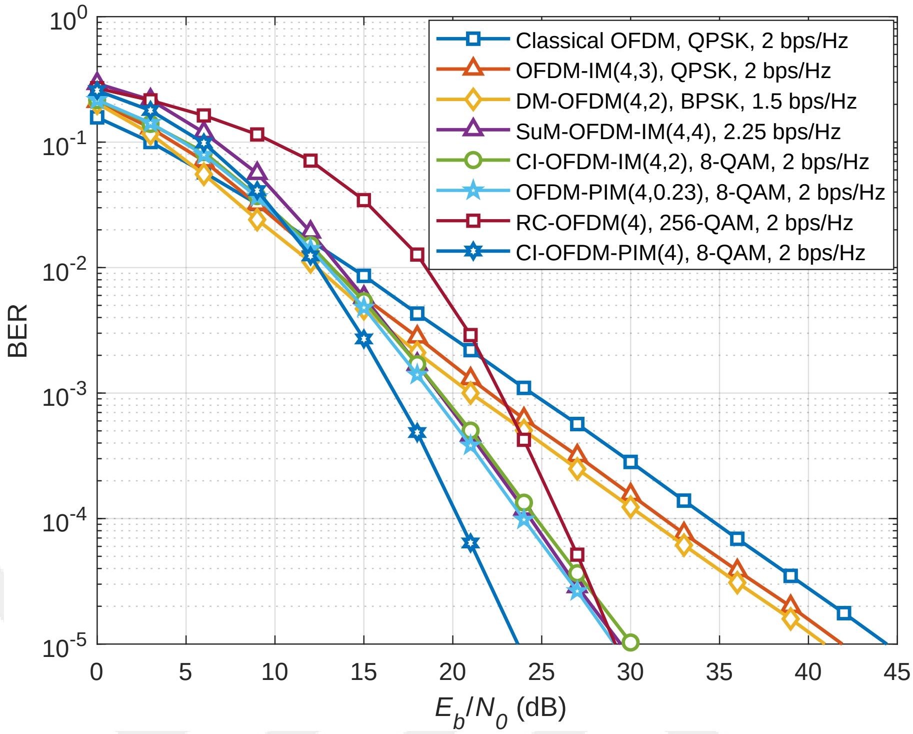

Figure 3.5: Error performance comparison of CI-OFDM-PIM with benchmark schemes.

RC-OFDM by using the ML detector. As seen from Fig. 3.5, CI-OFDM-PIM outperforms the other schemes in terms of error performance. At a BER value of 10^{-5}, CI-OFDM-PIM achieves approximately 6 dB gain over the closest rivals, which are CI-OFDM-IM, OFDM-PIM, RC-OFDM, and SuM-OFDM-IM.

Moreover, the error performance gap between CI-OFDM-PIM and the schemes with diversity order of 2 further extends as the SNR value increases thanks to its higher BER vs SNR slope caused by diversity order of 4.

Chapter 4

COORDINATE INTERLEAVED OFDM WITH REPEATED IN-PHASE/QUADRATURE INDEX MODULATION

OFDM-IM attracts much attention in the literature due to its several advantages such as high flexibility and implementation simplicity. Nonetheless, OFDM-IM cannot satisfy needs of future wireless communication services such as, superior reliability, high data rates, and low complexity. Thus, waveform designs which enhance the error performance and the spectral efficiency of OFDM-IM, should be designed.

CI-OFDM-RIQIM which is a novel OFDM-IM based system, provides a superior error performance and enhanced spectral efficiency compared to OFDM-IM due to its diversity order of two and clever SAP detection mechanism. Therefore, CI-OFDM-RIQIM is capable of providing a remarkable gain over OFDM-IM based tranmission schemes.

In this chapter, the system model including a low complexity LLR detector, performance analysis, and simulations results of CI-OFDM-RIQIM are presented, respectively.

4.1 System Model of CI-OFDM-RIQIM

CI-OFDM-RIQIM is an OFDM-based transmission system including a total number of N_F subcarriers. As seen from Fig. 4.1, a total number of B bits enter the system and these bits are then split into G groups of b bits, $b = B/G$. Each group of b bits is exploited to create an CI-OFDM-RIQIM subblock with size $N_S = N_F/G$, where N_s is an even number and greater than 2. Moreover, each subblock is divided into two clusters of length $N_C = N_S/2$. It is sufficient to investigate the formation of the ξ^{th} subblock $\mathbf{s}_\xi$, since the same processes are performed to

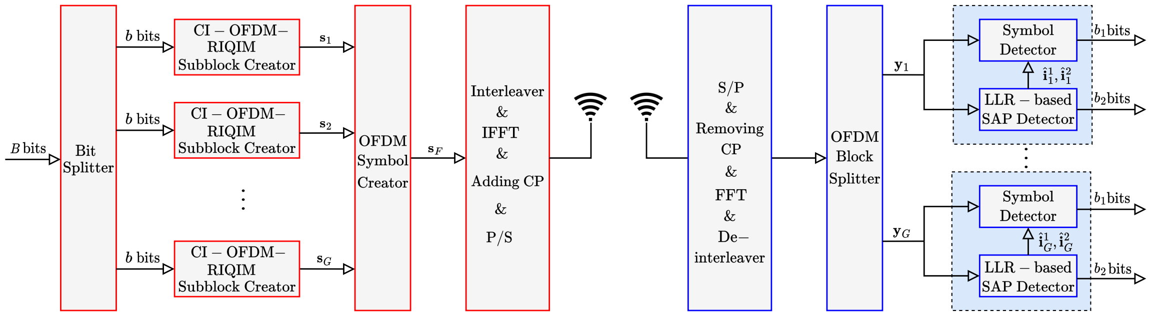

Figure 4.1: Transceiver architecture of CI-OFDM-RIQIM.

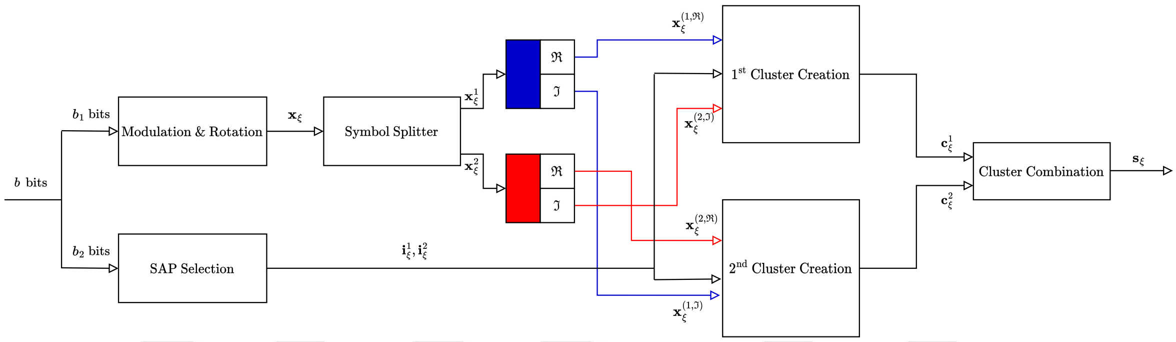

Figure 4.2: CI-OFDM-RIQIM Subblock Creator

constitute each subblock, where $\xi = 1, \cdots, G$. For the creation of $\mathbf{s}_\xi$, b bits are separated into two groups with b_1 and b_2 bits. Firstly, $b_1 = 2K \log_2 M$ bits determine the ξ^{th} data symbol vector $\mathbf{x}_\xi = [x_{\xi,1}, \cdots, x_{\xi,2K}]^{\text{T}}$, $x_{\xi,\kappa} \in \mathcal{M}^\theta$, $\kappa = 1, \cdots, 2K$, where K and $\mathcal{M}^\theta$ are the number of active subcarriers in a cluster and M-ary constellation rotated by an angle θ, respectively. Note that constellation rotation is a must to harvest diversity in CI-based schemes [Khan and Rajan, 2006]. Then, $\mathbf{x}_\xi$ is split into two parts: $\mathbf{x}_\xi^1 = [x_{\xi,1}, \cdots, x_{\xi,K}]$ and $\mathbf{x}_\xi^2 = [x_{\xi,K+1}, \cdots, x_{\xi,2K}]$, $\mathbf{x}_\xi = [(\mathbf{x}_\xi^1)^{\text{T}}, (\mathbf{x}_\xi^2)^{\text{T}}]^{\text{T}}$ and the real and imaginary parts of these vectors are obtained as $\mathbf{x}_\xi^1 = \mathbf{x}_\xi^{(1,\Re)} + j\mathbf{x}_\xi^{(1,\Im)}$ and $\mathbf{x}_\xi^2 = \mathbf{x}_\xi^{(2,\Re)} + j\mathbf{x}_\xi^{(2,\Im)}$. Secondly, by using combinatorial method or a look-up table [Başar et al., 2013], the λ^{th} subcarrier activation pattern (SAP), $\mathbf{i}_\xi^\lambda = [i_{\xi,1}^\lambda, \cdots, i_{\xi,K}^\lambda]^{\text{T}}$, $i_{\xi,k}^\lambda \in \{1, \cdots, N\}$, $k = 1, \cdots, K$, is selected by $b_2/2 = \lfloor \log_2 \binom{N_C}{K} \rfloor$ bits, where $\lambda = 1, 2$. Here, a total number of $b_2 = 2\lfloor \log_2 \binom{N_C}{K} \rfloor$ bits are transmitted via the selected SAPs $(\mathbf{i}_\xi^1, \mathbf{i}_\xi^2)$. Subsequently, the entries of $\mathbf{x}^{(1,R)}$

and $\mathbf{x}^{(2,\Im)}$ are inserted into the first cluster $\mathbf{c}_\xi^1 = [c_{\xi,1}^1, \cdots, c_{\xi,N_C}^1]$ with the entries of $\mathbf{i}_\xi^1$ and $\mathbf{i}_\xi^2$, respectively. Moreover, the entries of $\mathbf{x}^{(2,\Re)}$ and $\mathbf{x}^{(1,I)}$ are inserted into the second cluster $\mathbf{c}_\xi^2 = [c_{\xi,1}^2, \cdots, c_{\xi,N_C}^2]$ with the entries of $\mathbf{i}_\xi^2$ and $\mathbf{i}_\xi^1$, respectively. Then, the ξ^{th} subblock is obtained as $\mathbf{s}_\xi = [(\mathbf{c}_\xi^1)^{\mathrm{T}}, (\mathbf{c}_\xi^2)^{\mathrm{T}}]^{\mathrm{T}} = [s_{\xi,1}, \cdots, s_{\xi,N_S}]^{\mathrm{T}}$, where $s_{\xi,\mu} \in \{0, \mathcal{M}^{(\theta,\Re)}, j\mathcal{M}^{(\theta,\Im)}, \tilde{\mathcal{M}}\}$, $\mu = 1, \cdots, N_S$, $\mathcal{M}^{(\theta,\Re)}$ and $\mathcal{M}^{(\theta,\Im)}$ are the real and imaginary parts of the rotated constellation $\mathcal{M}^\theta$, respectively. Additionally, $\tilde{\mathcal{M}}$ is a M^2-ary constellation whose each element is in the form of $x_1^\Re + jx_2^\Im$, where $x_1^\Re \in \mathcal{M}^{(\theta,\Re)}$ and $x_2^\Im \in \mathcal{M}^{(\theta,\Im)}$. Hence, the number of bits transmitted by the ξ^{th} CI-OFDM-RIQIM subblock is expressed as:

$$b = 2K \log_2 M + 2\left\lfloor \log_2 \binom{N_C}{K} \right\rfloor. \tag{4.1}$$

Finally, by concatenating all subblocks, the overall transmitted OFDM symbol is obtained as $\mathbf{s}_F = [\mathbf{s}_1^{\mathrm{T}}, \cdots, \mathbf{s}_G^{\mathrm{T}}]^{\mathrm{T}}$. Note that in this scheme, CI is not directly applied to the data symbols as in [Başar, 2015]; however, after placing the data symbols into the subblock, a number of data symbols might be coordinate interleaved.

For better illustration, we provide a mapping example for the creation of all subblocks with specified parameters. Since the same processes are applied for each subblock, we remove the subscript ξ here. Assuming $N_C = 4$, $K = 2$, $N_S = 8$, all possible subblocks are presented in Table 4.1.

After forming the overall OFDM symbol by repeating the same procedure for all subblocks, a block-type interleaver is employed as in [Başar, 2015]. The time domain signal is acquired by taking inverse fast Fourier Transform (IFFT). After adding cyclic prefix (CP) with length L to the beginning of the OFDM frame and employing parallel to serial (P/S) and digital/analog transformation, the time-domain OFDM signal is transmitted through a T-tap frequency-selective Rayleigh fading channel with channel impulse response (CIR) coefficients

$$\mathbf{h}_T = [h_T(1) \cdots h_T(T)]^{\mathrm{T}}, \tag{4.2}$$

where $h_T(\beta), \beta = 1, \cdots, T$ follows circularly symmetric complex Gaussian random variables with the $\mathcal{CN}(0, 1/T)$.

At the receiver part, to obtain the signal in the frequency domain, first the CP is removed, and then FFT and deinterleaving are exploited. Finally, the equivalent

Table 4.1: All CI-OFDM-RIQIM Subblock Realizations For $N_C = 4$ And $K = 2$.

First	Second	$2^*(\mathbf{i}^1)^{\mathrm{T}}$	$2^*(\mathbf{i}^2)^{\mathrm{T}}$	Subblock ($\mathbf{s}^{\mathrm{T}}$)							
$b_2/2$ bits	$b_2/2$ bits			s_1	s_2	s_3	s_4	s_5	s_6	s_7	s_8
{0 0}	{0 0}	[1 3]	[1 3]	$x_1^{\mathfrak{R}} + jx_3^{\mathfrak{I}}$	0	$x_2^{\mathfrak{R}} + jx_4^{\mathfrak{I}}$	0	$x_3^{\mathfrak{R}} + jx_1^{\mathfrak{I}}$	0	$x_4^{\mathfrak{R}} + jx_2^{\mathfrak{I}}$	0
{0 0}	{0 1}	[1 3]	[2 4]	$x_1^{\mathfrak{R}}$	$jx_3^{\mathfrak{I}}$	$x_2^{\mathfrak{R}}$	$jx_4^{\mathfrak{I}}$	$jx_1^{\mathfrak{I}}$	$x_3^{\mathfrak{R}}$	$jx_2^{\mathfrak{I}}$	$x_4^{\mathfrak{R}}$
{0 0}	{1 0}	[1 3]	[1 4]	$x_1^{\mathfrak{R}} + jx_3^{\mathfrak{I}}$	0	$x_2^{\mathfrak{R}}$	$jx_4^{\mathfrak{I}}$	$x_3^{\mathfrak{R}} + jx_1^{\mathfrak{I}}$	0	$jx_2^{\mathfrak{I}}$	$x_4^{\mathfrak{R}}$
{0 0}	{1 1}	[1 3]	[2 3]	$x_1^{\mathfrak{R}}$	$jx_3^{\mathfrak{I}}$	$x_2^{\mathfrak{R}} + jx_4^{\mathfrak{I}}$	0	$jx_1^{\mathfrak{I}}$	$x_3^{\mathfrak{R}}$	$x_4^{\mathfrak{R}} + jx_2^{\mathfrak{I}}$	0
{0 1}	{0 0}	[2 4]	[1 3]	$jx_3^{\mathfrak{I}}$	$x_1^{\mathfrak{R}}$	$jx_4^{\mathfrak{I}}$	$x_2^{\mathfrak{R}}$	$x_3^{\mathfrak{R}}$	$jx_1^{\mathfrak{I}}$	$x_4^{\mathfrak{R}}$	$jx_2^{\mathfrak{I}}$
{0 1}	{0 1}	[2 4]	[2 4]	0	$x_1^{\mathfrak{R}} + jx_3^{\mathfrak{I}}$	0	$x_2^{\mathfrak{R}} + jx_4^{\mathfrak{I}}$	0	$x_3^{\mathfrak{R}} + jx_1^{\mathfrak{I}}$	0	$x_4^{\mathfrak{R}} + jx_2^{\mathfrak{I}}$
{0 1}	{1 0}	[2 4]	[1 4]	$jx_3^{\mathfrak{I}}$	$x_1^{\mathfrak{R}}$	0	$x_2^{\mathfrak{R}} + jx_4^{\mathfrak{I}}$	$x_3^{\mathfrak{R}}$	$jx_1^{\mathfrak{I}}$	0	$x_4^{\mathfrak{R}} + jx_2^{\mathfrak{I}}$
{0 1}	{1 1}	[2 4]	[2 3]	0	$x_1^{\mathfrak{R}} + jx_3^{\mathfrak{I}}$	$jx_4^{\mathfrak{I}}$	$x_2^{\mathfrak{R}}$	0	$x_3^{\mathfrak{R}} + jx_1^{\mathfrak{I}}$	$x_4^{\mathfrak{R}}$	$jx_2^{\mathfrak{I}}$
{1 0}	{0 0}	[1 4]	[1 3]	$x_1^{\mathfrak{R}} + jx_3^{\mathfrak{I}}$	0	$jx_4^{\mathfrak{I}}$	$x_2^{\mathfrak{R}}$	$x_3^{\mathfrak{R}} + jx_1^{\mathfrak{I}}$	0	$x_4^{\mathfrak{R}}$	$jx_2^{\mathfrak{I}}$
{1 0}	{0 1}	[1 4]	[2 4]	$x_1^{\mathfrak{R}}$	$jx_3^{\mathfrak{I}}$	0	$x_2^{\mathfrak{R}} + jx_4^{\mathfrak{I}}$	$jx_1^{\mathfrak{I}}$	$x_3^{\mathfrak{R}}$	0	$x_4^{\mathfrak{R}} + jx_2^{\mathfrak{I}}$
{1 0}	{1 0}	[1 4]	[1 4]	$x_1^{\mathfrak{R}} + jx_3^{\mathfrak{I}}$	0	0	$x_2^{\mathfrak{R}} + jx_4^{\mathfrak{I}}$	$x_3^{\mathfrak{R}} + jx_1^{\mathfrak{I}}$	0	0	$x_4^{\mathfrak{R}} + jx_2^{\mathfrak{I}}$
{1 0}	{1 1}	[1 4]	[2 3]	$x_1^{\mathfrak{R}}$	$jx_3^{\mathfrak{I}}$	$jx_4^{\mathfrak{I}}$	$x_2^{\mathfrak{R}}$	$jx_1^{\mathfrak{I}}$	$x_3^{\mathfrak{R}}$	$x_4^{\mathfrak{R}}$	$jx_2^{\mathfrak{I}}$
{1 1}	{0 0}	[2 3]	[1 3]	$jx_3^{\mathfrak{I}}$	$x_1^{\mathfrak{R}}$	$x_2^{\mathfrak{R}} + jx_4^{\mathfrak{I}}$	0	$x_3^{\mathfrak{R}}$	$jx_1^{\mathfrak{I}}$	$x_4^{\mathfrak{R}} + jx_2^{\mathfrak{I}}$	0
{1 1}	{0 1}	[2 3]	[2 4]	0	$x_1^{\mathfrak{R}} + jx_3^{\mathfrak{I}}$	$x_2^{\mathfrak{R}}$	$jx_4^{\mathfrak{R}}$	0	$x_3^{\mathfrak{R}} + jx_1^{\mathfrak{I}}$	$jx_2^{\mathfrak{I}}$	$x_4^{\mathfrak{R}}$
{1 1}	{1 0}	[2 3]	[1 4]	$jx_3^{\mathfrak{I}}$	$x_1^{\mathfrak{R}}$	$x_2^{\mathfrak{R}}$	$jx_4^{\mathfrak{I}}$	$x_3^{\mathfrak{R}}$	$jx_1^{\mathfrak{I}}$	$jx_2^{\mathfrak{I}}$	$x_4^{\mathfrak{R}}$
{1 1}	{1 1}	[2 3]	[2 3]	0	$x_1^{\mathfrak{R}} + jx_3^{\mathfrak{I}}$	$x_2^{\mathfrak{R}} + jx_4^{\mathfrak{I}}$	0	0	$x_3^{\mathfrak{R}} + jx_1^{\mathfrak{I}}$	0	$x_4^{\mathfrak{R}} + jx_2^{\mathfrak{I}}$

input-output relationship corresponding to ξ in the frequency domain can be given by

$$\mathbf{y}_\xi = \mathbf{S}_\xi \mathbf{h}_\xi + \mathbf{n}_\xi, \tag{4.3}$$

where $\mathbf{S}_\xi = \operatorname{diag}(\mathbf{s}_\xi)$, $\mathbf{y}_\xi$, $\mathbf{h}_\xi$, and $\mathbf{n}_\xi$ represent the transmitted signal, received signal vector, channel coefficients, and noise samples vector corresponding to the ξ^{th} subblock, respectively. The distributions of the elements of $\mathbf{n}_\xi$ and $\mathbf{h}_\xi$ are $\mathcal{CN}(0, N_0)$ and $\mathcal{CN}(0, 1)$, respectively, where N_0 is the noise variance.

The maximum-likelihood (ML) detection can be performed to detect the ξ^{th} subblock by utilizing the set $\mathcal{S} = \{\mathbf{s}_1, \mathbf{s}_2, \cdots, \mathbf{s}_{2^b}\}$ which contains all possible subblock realizations:

$$\hat{\mathbf{s}}_\xi = \arg\min_{\mathbf{s}_\xi \in \mathcal{S}} \|\mathbf{y}_\xi - \mathbf{S}_\xi \mathbf{h}_\xi\|^2. \tag{4.4}$$

Since the ML detector searches for all possible of SAPs and data symbols in a exhaustive manner, it becomes unfeasible to exploit this detector for higher values of N_S, K, and M. Thus, we also present an LLR-based detector for CI-OFDM-RIQIM to reduce the detection complexity.

4.1.1 Low-Complexity LLR Detector for CI-OFDM-RIQIM

The proposed LLR detector aims to detect the CI-OFDM-RIQIM symbol subblock-by-subblock. For simplicity, we remove the subscript ξ.

The inputs of Algorithm 1 are given as follows:

- New received signal vector that is equalized by zero-forcing (ZF) equalizer: $\bar{\mathbf{y}} = [\bar{y}_1, \cdots, \bar{y}_{N_S}]^{\mathrm{T}}$, $\bar{y}_\mu = y_\mu / h_\mu$, $\mu = 1, \cdots, N_S$.

- Four different constellation sets: $\mathcal{M}_1 = \{\mathcal{M}^{(\theta,\Re)}, \mathcal{M}^\star\}$, $\mathcal{M}_2 = \{\mathcal{M}^{(\theta,\Im)}, \mathcal{M}'\}$, $\mathcal{M}_3 = \{\mathcal{M}^{(\theta,\Im)}, \mathcal{M}'\}$, and $\mathcal{M}_4 = \{\mathcal{M}^{(\theta,\Re)}, \mathcal{M}'\}$, where $\mathcal{M}^\star$ and $\mathcal{M}'$ are the M^2-ary constellations whose elements are in the form of $x_1^{\Re} + jx_2^{\Im}$ and $x_2^{\Re} + jx_1^{\Im}$, respectively, $(x_1, x_2) \in \mathcal{M}^\theta$.

- A set including all legal SAPs: $\mathcal{I} = \{\mathbf{i}_1, \cdots, \mathbf{i}_{2^{b_2/2}}\}$

- Noise variance: N_0.

The major steps of Algorithm 1 are discussed as follows:

1. The log-likelihood (LL) value of the c^{th} subcarrier being a symbol from the constellation set $\mathcal{M}_1$ and being null, is calculated at lines 3 and 4, respectively.

2. The LL value of the $(c+N_C)^{\mathrm{th}}$ subcarrier being a symbol from the constellation set $\mathcal{M}_2$ and being null, is calculated at lines 5 and 6, respectively.

3. The LL value of the c^{th} subcarrier being a symbol from the constellation set $\mathcal{M}_3$ and being null, is calculated at lines 7 and 8, respectively.

4. The LL value of the $(c+N_C)^{\mathrm{th}}$ subcarrier being a symbol from the constellation set $\mathcal{M}_4$ and being null, is calculated at lines 9 and 10, respectively.

5. The calculated LL values are combined between lines (11-14). Note that $\mathbf{\Lambda}_\lambda(\chi, c)$ is the element located in the χ^{th} row and c^{th} column of the matrix $\mathbf{\Lambda}_\lambda$, $\lambda = 1, 2$.

Algorithm 1 Low-Complexity LLR-Based SAP Detector for CI-OFDM-RIQIM

Input: $\bar{\mathbf{y}}$, N_0, $\mathcal{M}_1$, $\mathcal{M}_2$, $\mathcal{M}_3$, $\mathcal{M}_4$, $\mathcal{I}$

Output: $\hat{\mathbf{i}}^1$, $\hat{\mathbf{i}}^2$

for $c = 1$ **to** N_C **do**
    for $\chi = 1$ **to** $M^2 + M$ **do**
        $\Delta^{\Re}_{(1,1)} = -\frac{|h(c)|^2}{N_0}|\bar{y}^{\Re}(c) - \mathcal{M}_1(\chi)|^2$
        $\Delta^{\Re}_{(1,2)} = -\frac{|h(c)|^2}{N_0}|\bar{y}^{\Re}(c)|^2$
        $\Delta^{\Im}_{(2,1)} = -\frac{|h(N_C+c)|^2}{N_0}|\bar{y}^{\Im}(N_C + c) - \mathcal{M}_2(\chi)|^2$
        $\Delta^{\Im}_{(2,2)} = -\frac{|h(N_C+c)|^2}{N_0}|\bar{y}^{\Im}(N_C + c)|^2$
        $\Delta^{\Im}_{(1,1)} = -\frac{|h(c)|^2}{N_0}|\bar{y}^{\Im}(c) - \mathcal{M}_3(\chi)|^2$
        $\Delta^{\Im}_{(1,2)} = -\frac{|h(c)|^2}{N_0}|\bar{y}^{\Im}(c)|^2$
        $\Delta^{\Re}_{(2,1)} = -\frac{|h(N_C+c)|^2}{N_0}|\bar{y}^{\Re}(N_C + c) - \mathcal{M}_4(\chi)|^2$
        $\Delta^{\Re}_{(2,2)} = -\frac{|h(N_C+c)|^2}{N_0}|\bar{y}^{\Re}(N_C + c)|^2$
        $\mathbf{\Lambda}_1(\chi, c) = \Delta^{\Re}_{(1,1)} - \Delta^{\Re}_{(1,2)} + \Delta^{\Im}_{(2,1)} - \Delta^{\Im}_{(2,2)}$
        $\mathbf{\Lambda}_1(\chi, c) = \mathbf{\Lambda}_1(\chi, c) + \log(K) - \log(N_C - K)$
        $\mathbf{\Lambda}_2(\chi, c) = \Delta^{\Im}_{(1,1)} - \Delta^{\Im}_{(1,2)} + \Delta^{\Re}_{(2,1)} - \Delta^{\Re}_{(2,2)}$
        $\mathbf{\Lambda}_2(\chi, c) = \mathbf{\Lambda}_2(\chi, c) + \log(K) - \log(N_C - K)$
    end for
    $\Xi_1 = \mathbf{\Lambda}_1(1, c)$
    $\Xi_2 = \mathbf{\Lambda}_2(1, c)$
    for $\chi = 2$ **to** $M^2 + M$ **do**
        $\psi_1 = \log(1 + \exp(-|\Xi_1 - \mathbf{\Lambda}_1(\chi, c)|))$
        $\psi_2 = \log(1 + \exp(-|\Xi_2 - \mathbf{\Lambda}_2(\chi, c)|))$
        $T_1 = \max(\Xi_1, \mathbf{\Lambda}_1(\chi, c)) + \psi_1$
        $T_2 = \max(\Xi_2, \mathbf{\Lambda}_2(\chi, c)) + \psi_2$
        $\Xi_1 = T_1$
        $\Xi_2 = T_2$
    end for
    $\Omega_1(c) = \Xi_1$
    $\Omega_2(c) = \Xi_2$
end for
for $\beta = 1$ **to** $2^{b_2/2}$ **do**
    $\Omega'_1(\beta) = \sum_k \Omega_1(\mathcal{I}_\beta(k))$
    $\Omega'_2(\beta) = \sum_k \Omega_2(\mathcal{I}_\beta(k))$
end for
$\hat{\mathbf{i}}^1 = \mathcal{I}_{\max(\Omega'_1)}$
$\hat{\mathbf{i}}^2 = \mathcal{I}_{\max(\Omega'_2)}$

6. The joint LLR value corresponding to the c^{th} subcarrier of cluster 1 and 2 is calculated between lines (16-27).

7. The LLR values are combined according to the legal SAPs between lines (29-32). Note that $\mathcal{I}_\beta(k)$ represents the k^{th} element of the β^{th} SAP.

8. The detected SAPs $(\hat{\mathbf{i}}^1, \hat{\mathbf{i}}^2)$ are provided between lines (33-34). Note that the function $\max(\breve{\Omega}_\lambda)$ gives the index of the maximum value of $\breve{\Omega}_\lambda$.

After obtaining $(\hat{\mathbf{i}}^1, \hat{\mathbf{i}}^2)$, the equivalent model as in [Başar, 2015] is exploited to detect the k^{th} data symbol corresponding to the λ^{th} half of the data symbol vector $\mathbf{x}^\lambda$ as follows:

$$\hat{x}_k^\lambda = \min_{x \in \mathcal{M}^\theta} \|\breve{\mathbf{y}}_k^\lambda - \breve{\mathbf{H}}_k^\lambda [x^{\Re} \; x^{\Im}]^{\mathrm{T}}\|^2, \tag{4.5}$$

where $\breve{\mathbf{y}}_k^\lambda$ and $\breve{\mathbf{H}}_k^\lambda$ are given in (4.6) and (4.7), repectively for $\lambda = 1, 2$.

$$\breve{\mathbf{y}}_k^\lambda = \begin{bmatrix} \mathbf{y}^{\Re}(\hat{\mathbf{i}}^\lambda(k)) \\ \mathbf{y}^{\Im}(\hat{\mathbf{i}}^\lambda(k)) \\ \mathbf{y}^{\Re}(\hat{\mathbf{i}}^\lambda(k) + N_C) \\ \mathbf{y}^{\Im}(\hat{\mathbf{i}}^\lambda(k) + N_C) \end{bmatrix} \tag{4.6}$$

$$\breve{\mathbf{H}}_k^1 = \begin{bmatrix} \mathbf{h}^{\Re}(\hat{\mathbf{i}}^1(k)) & 0 \\ \mathbf{h}^{\Im}(\hat{\mathbf{i}}^1(k)) & 0 \\ 0 & -\mathbf{h}^{\Im}(\hat{\mathbf{i}}^1(k) + N_C) \\ 0 & \mathbf{h}^{\Re}(\hat{\mathbf{i}}^1(k) + N_C) \end{bmatrix}, \breve{\mathbf{H}}_k^2 = \begin{bmatrix} 0 & -\mathbf{h}^{\Im}(\hat{\mathbf{i}}^2(k)) \\ 0 & \mathbf{h}^{\Re}(\hat{\mathbf{i}}^2(k)) \\ \mathbf{h}^{\Re}(\hat{\mathbf{i}}^2(k) + N_C) & 0 \\ \mathbf{h}^{\Im}(\hat{\mathbf{i}}^2(k) + N_C) & 0 \end{bmatrix}. \tag{4.7}$$

4.2 Performance Analysis

In this section, we derive the theoretical upper bound of the bit error probability (BEP) for the proposed schemes. In addition, we analyze the diversity order of the proposed schemes. Furthermore, an optimization strategy on the θ value is given to minimize the BER, resulting in superior error performance.

4.2.1 Theoretical Upper Bound on BEP

In this subsection, an upper bound for the BEP of the proposed schemes is derived by employing ML detection. By utilizing (4.4), the conditional pairwise error probability (CPEP) which can be defined as the probability of erroneously detecting $\hat{\mathbf{S}}$ while transmitting $\mathbf{S}$ conditioned on $\mathbf{h}$, is expressed as:

$$\mathrm{P}(\mathbf{S} \rightarrow \hat{\mathbf{S}}|\mathbf{h}) = \mathrm{Q}\left(\sqrt{\frac{\phi}{2}\left|\left|(\mathbf{S}-\hat{\mathbf{S}})\mathbf{h}\right|\right|^2}\right). \tag{4.8}$$

Then, by taking the approximation of $\mathrm{Q}(x) \approx \frac{e^{-2x^2/3}}{4} + \frac{e^{-x^2/2}}{12}$ into consideration, the unconditioned PEP (UPEP) can be derived as in [Başar et al., 2013]:

$$\begin{aligned}\mathrm{P}(\mathbf{S} \rightarrow \hat{\mathbf{S}}) &= E_{\mathbf{h}}\{\mathrm{P}(\mathbf{S} \rightarrow \hat{\mathbf{S}}|\mathbf{h})\} \\ &\approx \frac{1/4}{\det(\mathbf{I}_{N_S}+\phi_1\mathbf{A})} + \frac{1/12}{\det(\mathbf{I}_{N_S}+\phi_2\mathbf{A})},\end{aligned} \tag{4.9}$$

where $\phi_1 = 1/3N_0$, $\phi_2 = 1/4N_0$, and $\mathbf{A} = (\mathbf{S}-\hat{\mathbf{S}})^{\mathrm{H}}(\mathbf{S}-\hat{\mathbf{S}})$ is the $N_s \times N_s$ difference matrix. Then, the BER of the CI-OFDM-RIQIM can be upper bounded by:

$$P_b \leq \frac{1}{b2^b}\sum_{\mathbf{S}}\sum_{\hat{\mathbf{S}}}\mathrm{P}(\mathbf{S} \rightarrow \hat{\mathbf{S}})\mathrm{e}(\mathbf{S},\hat{\mathbf{S}}), \tag{4.10}$$

where $\mathrm{e}(\mathbf{S},\hat{\mathbf{S}})$ is the number of faulty bits when $\mathbf{S}$ is transmitted, but erroneously detected as $\hat{\mathbf{S}}$.

4.2.2 Diversity Analysis

In this subsection, we investigate the diversity order of CI-OFDM-RIQIM by considering two cases: (a) erroneous detection of index bits while data symbols are correctly decoded and (b) erroneous detection of single or multiple data symbols while index bits are correctly decoded. For case (a), assume that subblock $\mathbf{s}$ with the parameters $(\mathrm{i}^1)^{\mathrm{T}} = [1,3]$ and $(\mathrm{i}^2)^{\mathrm{T}} = [1,3]$ is transmitted; however, subblock $\hat{\mathbf{s}}$ with the parameters $(\mathrm{i}^1)^{\mathrm{T}} = [1,3]$ and $(\hat{\mathrm{i}}^2)^{\mathrm{T}} = [1,4]$ is erroneously decoded for the given parameters $N_C = 4$ and $K = 2$ while data symbols are correctly decoded.

This error event can be expressed as:

$$\mathbf{s} \to \hat{\mathbf{s}} = [x_1^{\mathfrak{R}} + jx_3^{\mathfrak{I}}, 0, x_2^{\mathfrak{R}} + jx_4^{\mathfrak{I}}, 0 | x_3^{\mathfrak{R}} + jx_1^{\mathfrak{I}}, 0, x_4^{\mathfrak{R}} + jx_2^{\mathfrak{I}}, 0]$$
$$\to [x_1^{\mathfrak{R}} + jx_3^{\mathfrak{I}}, 0, x_2^{\mathfrak{R}}, jx_4^{\mathfrak{I}} | x_3^{\mathfrak{R}} + jx_1^{\mathfrak{I}}, 0, jx_2^{\mathfrak{I}}, x_4^{\mathfrak{R}}]. \tag{4.11}$$

This specific example is the worst case event and provides a diversity order of $\Gamma = 2$, where $\Gamma = \text{rank}(\mathbf{A})$. For case (b), assume that subblock $\mathbf{s}$ with data symbols (x_1, x_2, x_3, x_4), is transmitted; however, subblock $\hat{\mathbf{s}}$ with a single symbol error $(\hat{x_1}, x_2, x_3, x_4)$, is erroneously decoded while indices $(\mathrm{i}^1)^{\mathrm{T}} = [1, 3]$ and $(\mathrm{i}^2)^{\mathrm{T}} = [1, 3]$ are correctly detected, $N_C = 4$, and $K = 2$. This error event can be stated as:

$$\mathbf{s} \to \hat{\mathbf{s}} = [x_1^{\mathfrak{R}} + jx_3^{\mathfrak{I}}, 0, x_2^{\mathfrak{R}} + jx_4^{\mathfrak{I}}, 0 | x_3^{\mathfrak{R}} + jx_1^{\mathfrak{I}}, 0, x_4^{\mathfrak{R}} + jx_2^{\mathfrak{I}}, 0]$$
$$\to [\hat{x}_1^{\mathfrak{R}} + jx_3^{\mathfrak{I}}, 0, x_2^{\mathfrak{R}} + jx_4^{\mathfrak{I}}, 0 | x_3^{\mathfrak{R}} + j\hat{x}_1^{\mathfrak{I}}, 0, x_4^{\mathfrak{R}} + jx_2^{\mathfrak{I}}, 0]. \tag{4.12}$$

As seen from (4.12), even erroneous detection of a single data symbol causes changes over two separated subcarriers and; thus, a diversity order of $\Gamma = 2$ is guaranteed. Eventually, the proposed schemes ensure $\min_{\mathbf{S},\hat{\mathbf{S}}}(\Gamma) = 2$, which proves that the diversity order of CI-OFDM-RIQIM and is 2.

Moreover, total numbers of error events that have a rank value of $\Gamma = 2, 3, 4, 5, 6, 7$ and 8, are presented in Fig. 4.3 to give further insight about the performance of the proposed scheme for $N_S = 8$ at a spectral efficiency of 1.25 bps/Hz. As it can be concluded from from Fig. 4.3, CI-OFDM-RIQIM provides more error events with $\Gamma = 8$ compared to RIM-OFDM-CI and CI-OFDM-IM, resulting in superior error performance.

4.2.3 Optimization

In this subsection, we find the optimum θ value which minimizes the BER by searching θ values from 1° to 89°. with increments of 1°. Note that since quadrature amplitude modulation (QAM) constellation repeats itself every 90°, we do not examine beyond this angle. The angle that provides the lowest BER at a selected SNR value, is selected as the optimum angle for the system. For example, as seen in Fig. 4.4, with the given parameters $N_c = 4$ and $K = 2$, the optimum θ for CI-OFDM-RIQIM

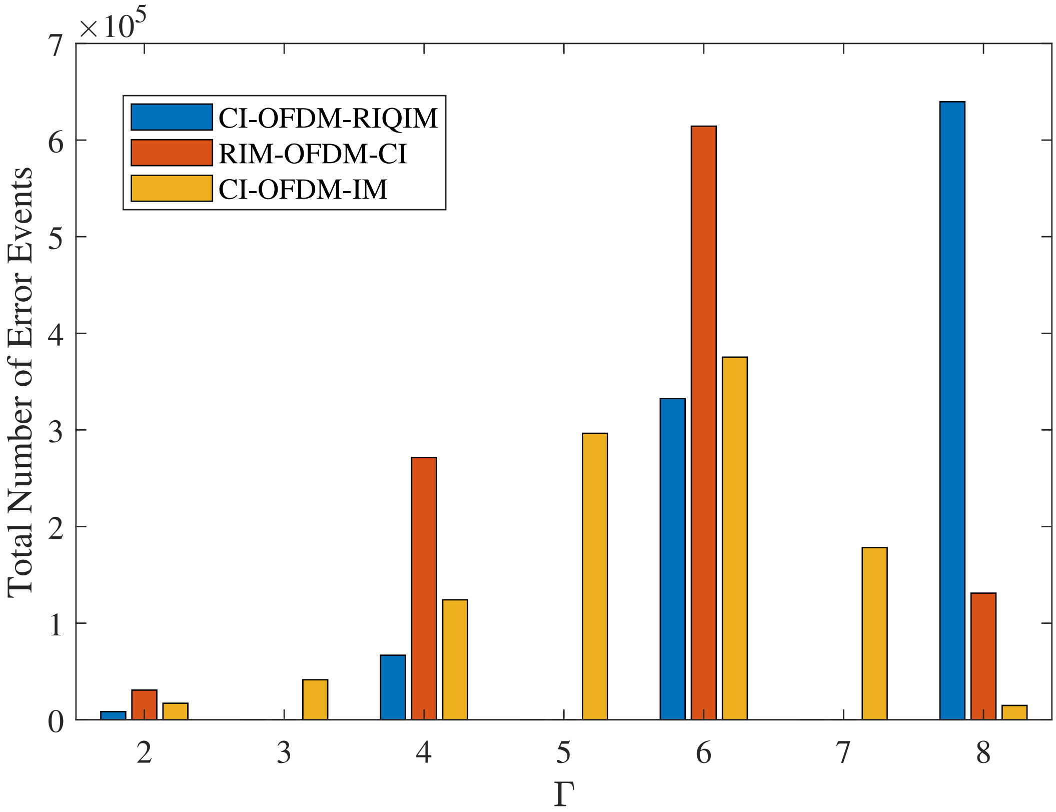

Figure 4.3: Total number of error events with $\Gamma = 2, \cdots, 8$ for CI-OFDM-RIQM and benchmark schemes.

system is obtained as 63° and 22° for 4-QAM and 8-QAM, respectively, when SNR is fixed to 15 dB. Moreover, we use the proposed LLR detectors to find an optimum rotation angle for higher modulation orders since it is not feasible to determine the optimum angle by employing ML detection. For instance, θ is obtained as 72° and 18° for 16-QAM and 64-QAM, respectively as seen from Fig. 4.5.

4.3 Simulation Results And Comparisons

In this section, CI-OFDM-RIQIM is compared with various OFDM-IM based reference schemes via computer simulations, given that all simulations are realized with the system parameters of $N_F = 128$, $L = 16$, and $T = 10$ tap Rayleigh fading channel. For the sake of simplicity, we will define "OFDM-IM (N_S,K,M)", "OFDM-IQ-IM (N_S,K,M)", "CI-OFDM-IM (N_S,K,M)", and "ReMO (N_S,K,M)" as OFDM-

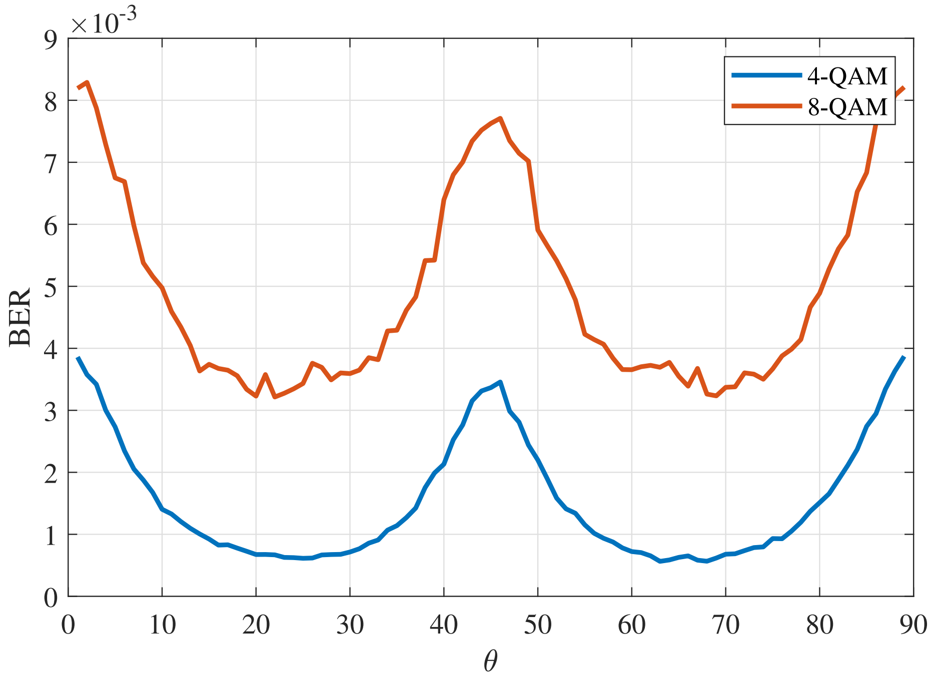

Figure 4.4: Optimum rotation angle search for 4-QAM and 8-QAM using ML detector when SNR is fixed to 15 dB.

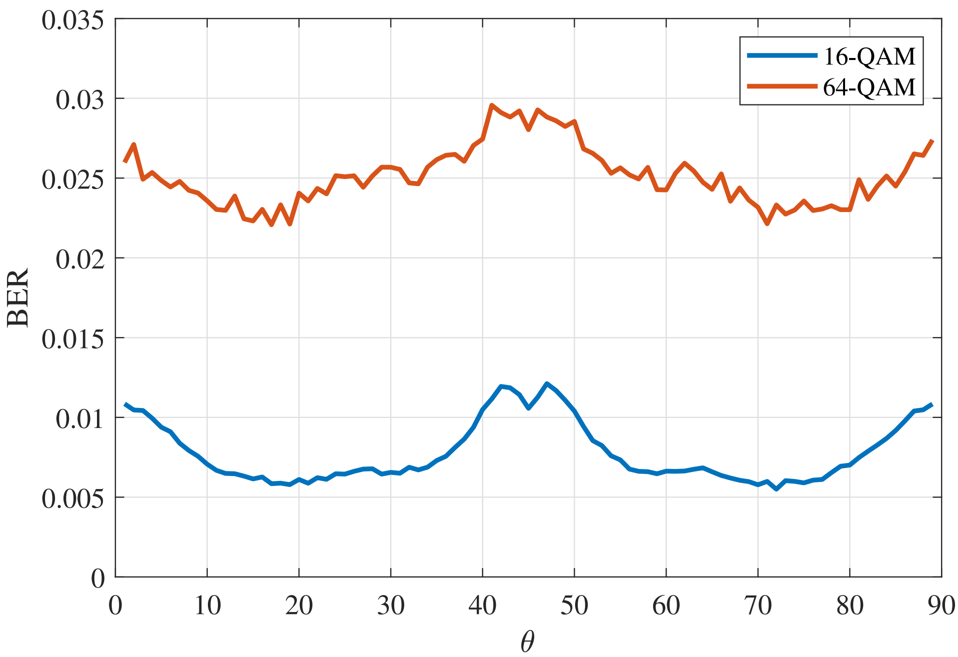

Figure 4.5: Optimum rotation angle search for 16-QAM and 64-QAM using LLR detector, when SNR is fixed to 15 dB.

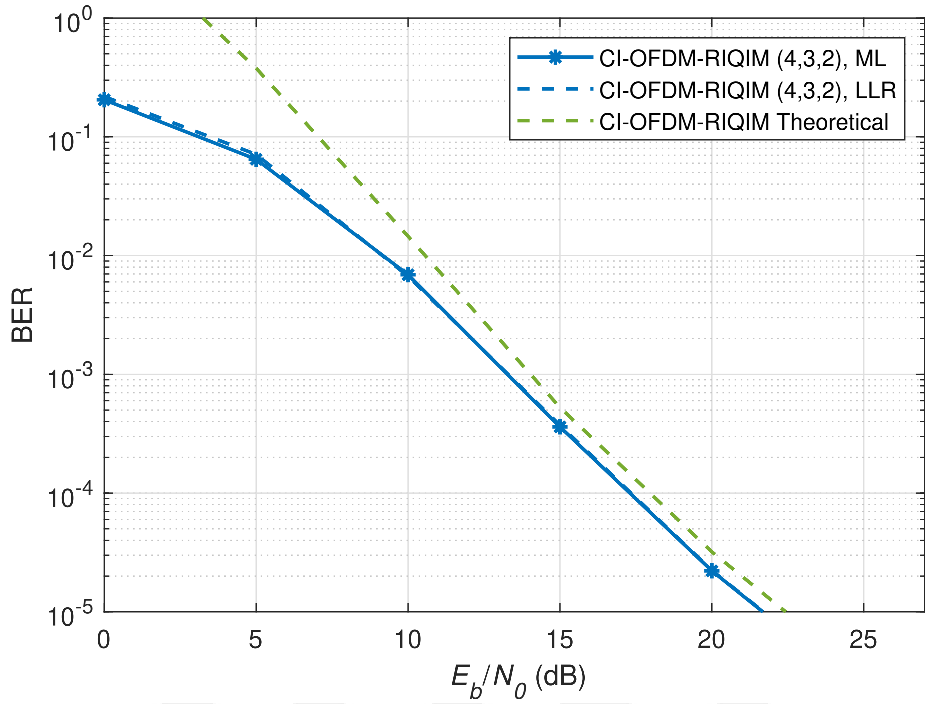

Figure 4.6: Error performance of CI-OFDM-RIQIM for the cases where ML and LLR detectors are utilized at a spectral efficiency of 1.25 bps/Hz.

IM, OFDM-IQ-IM, CI-OFDM-IM, and ReMO schemes, respectively, where K out of N_S subcarriers are activated in one subblock and M is the modulation order. Moreover, we will refer to "RIM-OFDM-CI (N_C,K,M)" and "CI-OFDM-RIQIM (N_C,K,M)" as RIM-OFDM-CI and CI-OFDM-RIQIM schemes, respectively, where K subcarriers are active in one cluster with size N_C while M is the modulation order. Note that optimum rotation angles for simulations of the proposed schemes have been determined based on the optimization strategy explained in Section III.

As shown in Fig. 4.6, theoretical BER curve that are acquired by (4.10), is an accurate upper bound for CI-OFDM-RIQIM. In addition, as seen in Fig. 4.6, the proposed LLR detector for CI-OFDM-RIQIM have considerable close error performance compared to the BER performance obtained by ML detector while having reduced complexity.

As seen from Fig. 4.7, CI-OFDM-RIQIM provides superior error performance compared to the benchmark schemes at a spectral efficiency of 1 bps/Hz. CI-OFDM-

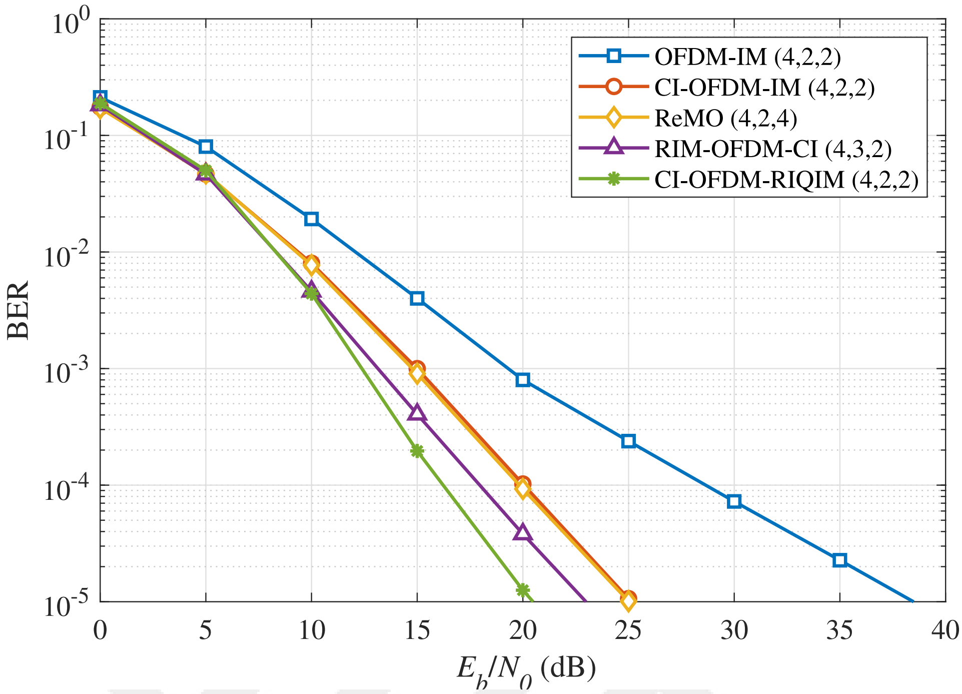

Figure 4.7: Error performance comparison of CI-OFDM-RIQIM with benchmark schemes at a spectral efficiency of 1 bps/Hz.

RIQIM has approximately 3 dB, 5 dB and 17 dB SNR gain over RIM-OFDM-CI, CI-OFDM-IM, and OFDM-IM, respectively, although less number of subcarriers are activated in one cluster due to the increased number of transmitted IM bits.

In Fig. 4.8, the error performance of CI-OFDM-RIQIM and reference schemes is investigated at a spectral efficiency of 1.25 bps/Hz. It is observed that CI-OFDM-RIQIM outperforms all benchmark schemes in terms of error performance. Furthermore, CI-OFDM-RIQIM provides almost a 4 dB gain over the nearest benchmark while utilizing a lower modulation order due to the doubled number of IM bits.

Fig. 4.9 shows an error performance comparison between the proposed and benchmark schemes, where the subblock size is four. It can be deduced from Fig. 4.9 that, CI-OFDM-RIQIM show slightly better error performance compared to RIM-OFDM-CI and CI-OFDM-IM while its spectral efficiency value is 14.3% higher.

In Fig. 4.10, CI-OFDM-RIQIM and the benchmark schemes are compared in terms of BER performance when spectral efficiency is 2.75 bps/Hz, $N_S = 8$, and LLR detectors are employed in all simulations. As seen from Fig. 4.10, approximately a 5

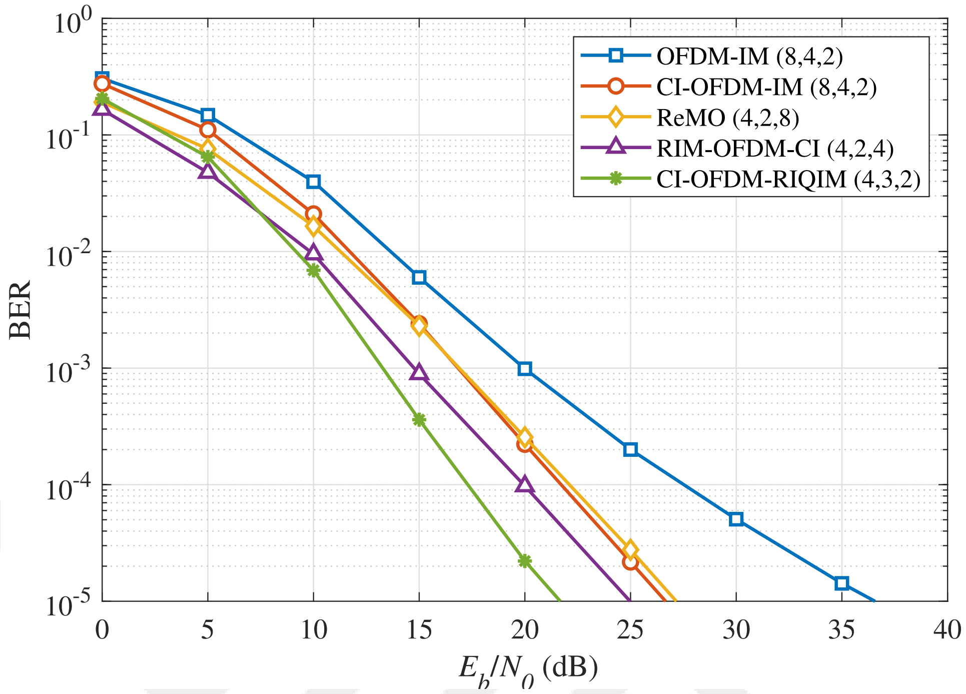

Figure 4.8: Error performance comparison of CI-OFDM-RIQIM with benchmark schemes at a spectral efficiency of 1.25 bps/Hz.

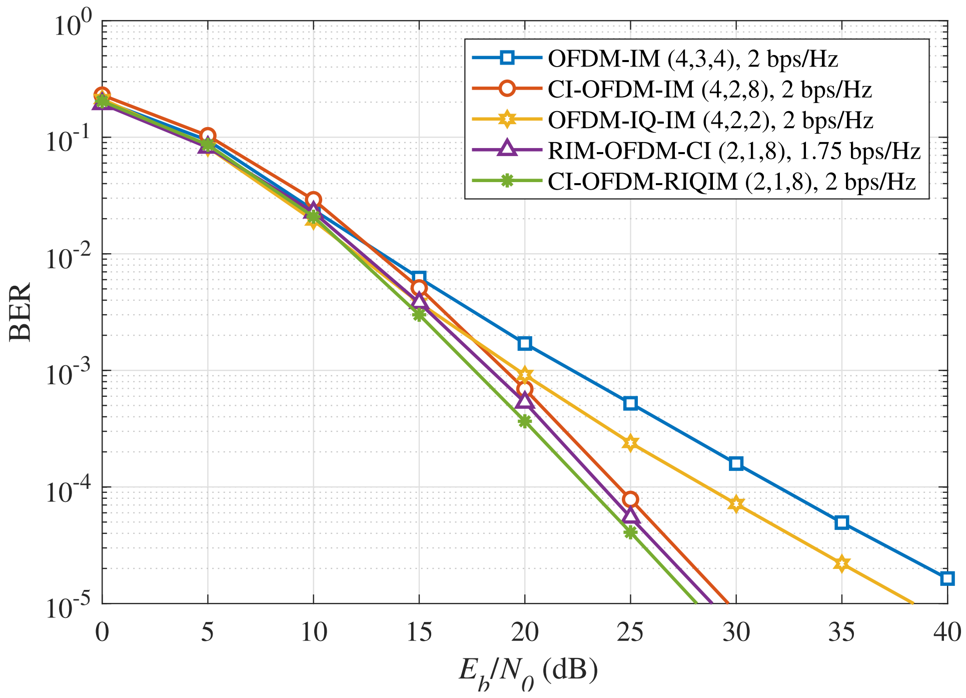

Figure 4.9: Error performance comparison of CI-OFDM-RIQIM with benchmark schemes.

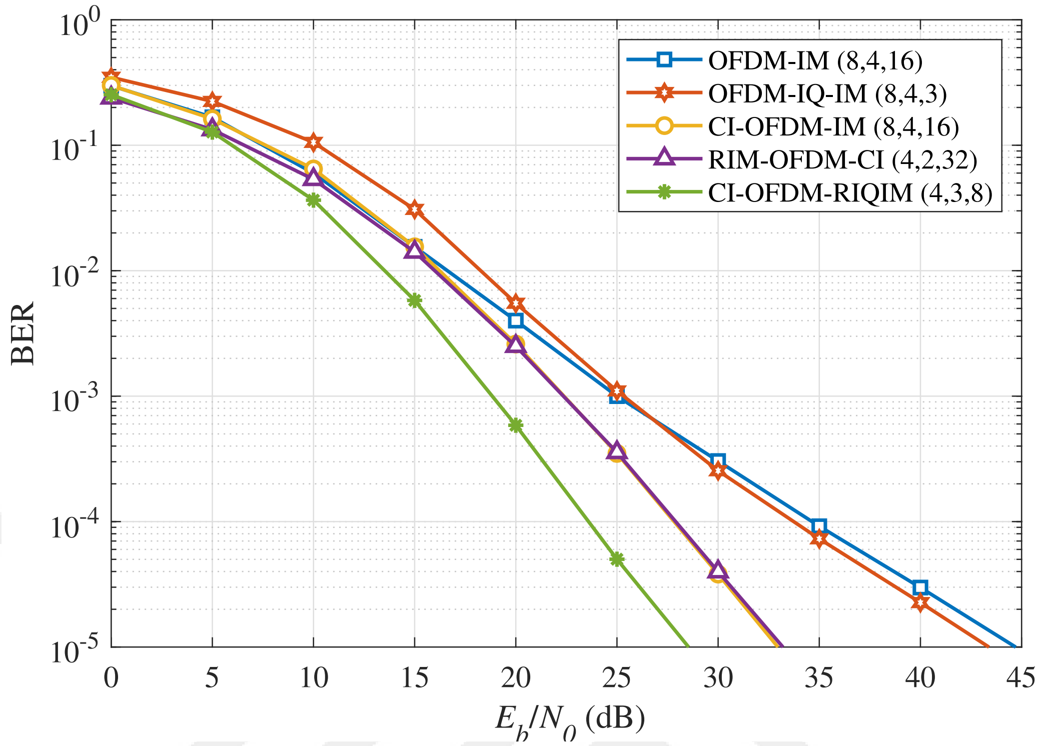

Figure 4.10: Error performance comparison of CI-OFDM-RIQIM with benchmark schemes when at a spectral efficiency of 2.75 bps/Hz by utilizing LLR detectors.

dB gain over RIM-OFDM-CI and CI-OFDM-IM is provided by CI-OFDM-RIQIM at a BER value of 10^{-5}. Furthermore, the same spectral efficiency is obtained by lower modulation order in CI-OFDM-RIQIM, resulting in enhanced error performance.

Error performance of CI-OFDM-RIQIM for varying cluster sizes are investigated using LLR detectors in Fig. 4.11 where the spectral efficiency is 2.5 bps/Hz. As N_C increases, higher rank values are obtained more frequently and this explains the reason why CI-OFDM-RIQIM with higher subblock size outperforms other cases as seen from Fig. 4.11.

While previous simulation results assume perfect CSI, the error performance of the proposed and existing schemes which also provide diversity order of two, is compared under the imperfect CSI conditions, in Fig. 4.12. For this, ML detection is performed by estimating $\hat{\mathbf{H}} = \mathrm{diag}\{\hat{h}_1, \cdots, \hat{h}_{N_S}\}$ instead of the true $\mathbf{H}$ in (4.3) to decode the transmitted signal as in [Van Luong et al., 2018]. It is assumed that

$$\mathbf{H} = \hat{\mathbf{H}} + \mathbf{E}, \tag{4.13}$$

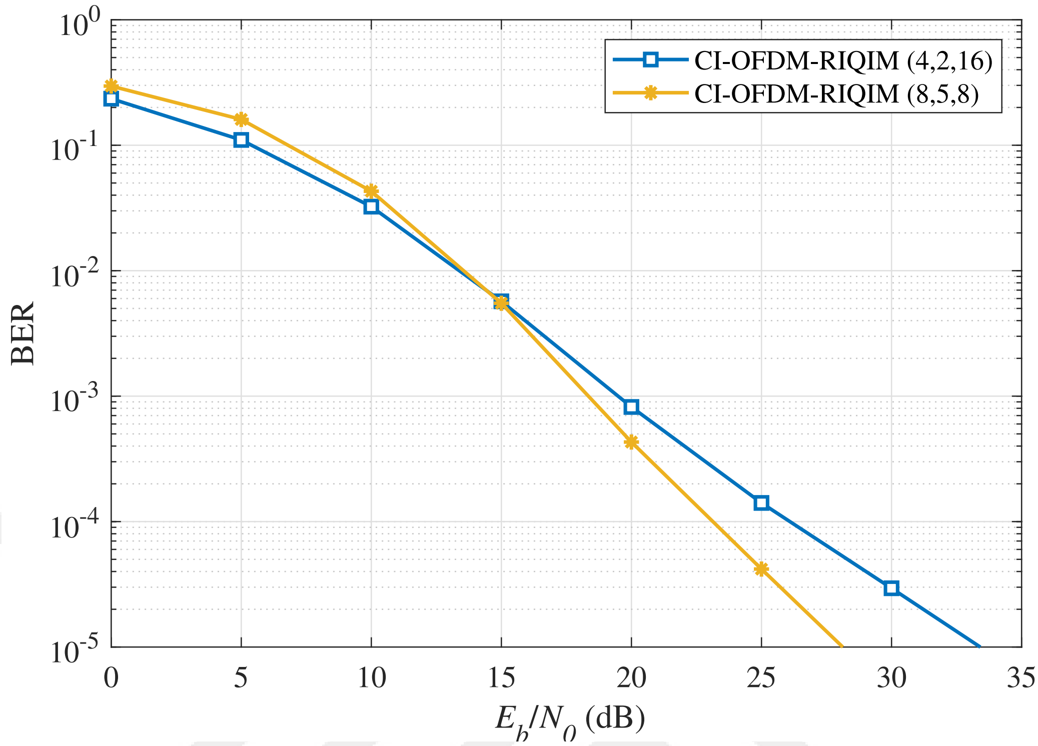

Figure 4.11: Error performance comparison of CI-OFDM-RIQIM for varying parameters at a spectral efficiency of 2.5 bps/Hz.

where $\mathbf{E} = \text{diag}\{e_1, \cdots, e_{N_S}\}$ denotes the matrix of channel estimation errors, whose elements follow $e_\alpha \sim \mathcal{CN}(0, \epsilon^2)$, $\alpha = 1, \cdots, N_S$, and ϵ^2 is the error variance where $\epsilon^2 \in [0, 1)$. Then, elements of the $\hat{\mathbf{H}}$ satisfies $\hat{h}_\alpha \sim \mathcal{CN}(0, 1 - \epsilon^2)$. Therefore, we obtain

$$h_\alpha = \hat{h}_\alpha + e_\alpha \tag{4.14}$$

for each sub-channel. Moreover, simulations in Fig. 4.12 are realized under the fixed CSI conditions with $\epsilon^2 = 0.05$ and $\epsilon^2 = 0.01$. As observed from Fig. 4.12, proposed scheme still outperforms the reference schemes. For example, at a BER value of 10^{-2} and $\epsilon^2 = 0.01$, CI-OFDM-RIQIM provides approximately 1 dB and 3 dB SNR gain over RIM-OFDM-CI and CI-OFDM-IM, respectively.

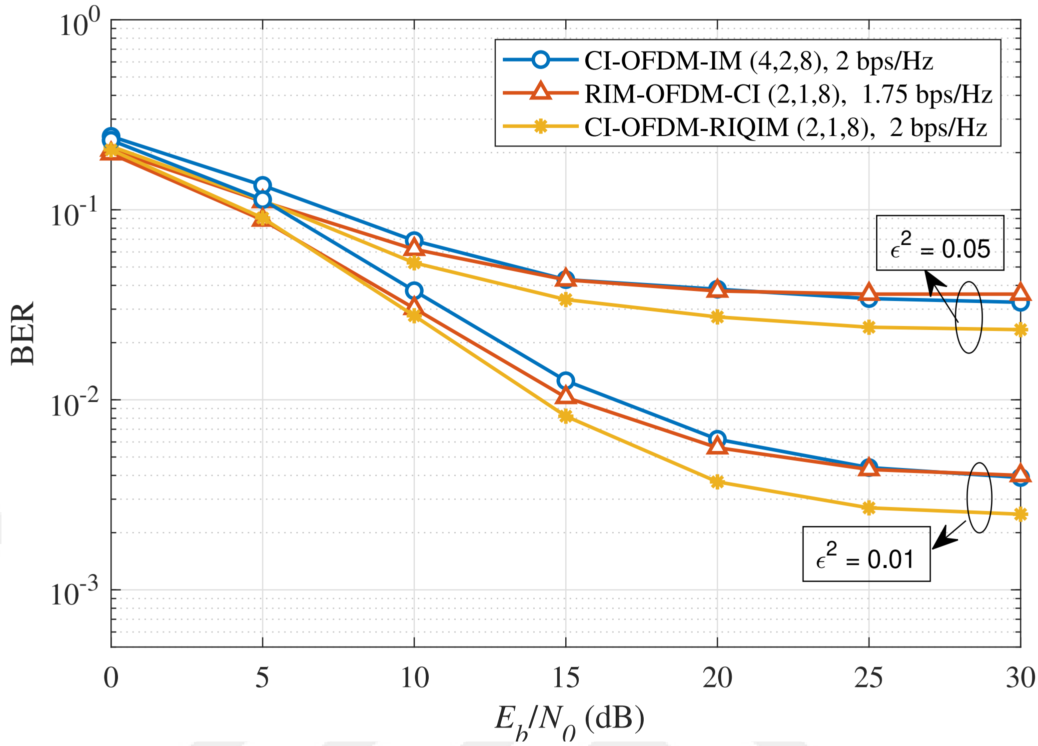

Figure 4.12: Error performance comparison of CI-OFDM-RIQIM with benchmark schemes under the imperfect CSI conditions for the parameters of $\epsilon^2 = 0.05$ and $\epsilon^2 = 0.01$.

4.3.1 Complexity Analysis

In Table 4.2, an analysis in terms of the complexity order of the low complexity LLR-based detectors of the proposed and benchmark schemes is given. As seen from Table 4.2, detection complexity of the CI-OFDM-RIQIM increasing exponentially.

To further investigate the complexity comparison between the proposed and reference schemes, we provide a numerical example. For a fair comparison, parameters in Fig. 4.8 are considered. Since the spectral efficiency and the subblock sizes are equal for all schemes, the total number of complex multiplications (CMs) per subcarrier is 128 for all schemes when ML detector is employed. As it can be deduced from Table 4.2, the total number of CMs per subcarrier is dramatically reduced by proposed LLR detector. For example, a total number of 16 CMs per subcarrier is sufficient for spectral efficiencies of 2 and 2.75 dB. Besides, we obtain an interesting trade-off between our proposed and benchmark schemes in terms of complexity

Table 4.2: Complexity Comparison of LLR Detectors.

System	Complexity Order
OFDM-IM	$\mathcal{O}(M)$
CI-OFDM-IM	$\mathcal{O}(M^2)$
RIM-OFDM-CI	$\mathcal{O}(M^2)$
CI-OFDM-RIQIM	$\mathcal{O}(M^2)$

and error performance. Although, CI-OFDM-RIQIM is the third complex system for these spesific parameters, it provides superior error performance compared to benchmark schemes as seen from Fig. 4.10.

Chapter 5

CONCLUSION

In this thesis, we have proposed two novel OFDM-IM based multicarrier transmission scheme to meet the diverse needs of next generation communication services.

First, a novel OFDM-IM based transmission scheme called CI-OFDM-PIM is proposed. CI-OFDM-PIM provides remarkable error performance by benefiting from CI and power distribution. CI-OFDM-PIM outperforms its benchmarks with a diversity order of 2 such as CI-OFDM-IM, OFDM-PIM and RC-OFDM by 6 dB gain due to its superior diversity gain which is equal to the number of subcarriers in each subblock. CI-OFDM-PIM can have a great potential for next generation wireless networks thanks to its advantages such as outstanding BER performance and high diversity gain.

Secondly, another novel diversity achieving OFDM-IM based transmission scheme called CI-OFDM-RIQIM, which first divides all subblocks into two clusters and transmits real and imaginary parts of the data symbols over the active subcarriers in these clusters, is proposed. Moreover, an LLR-based detector have been designed for the proposed scheme to reduce the overall system complexity. Finally, the error performance of the proposed scheme have been investigated by computer simulations. We conclude that CI-OFDM-RIQIM noticeably outperforms the reference schemes since data bits conveyed by IM are increased. In addition, designed LLR detector noticeably reduces the detection complexity while still providing superior error performances. Eventually, additional diversity gain, remarkable error performance, and higher spectral efficiency make the CI-OFDM-RIQIM based schemes appropriate candidates for next generation communication services.

In conclusion, our proposed schemes can be considered as proper multicarrier transmission techniques for future wireless communication systems. However, these schemes can be further extended by employing other decoding/encoding techniques, enhancing spectral efficiency, and improving reliability. In addition, proposed methods can be enriched by real time experiments and practical implementations. Moreover, the generalization of CI-OFDM-PIM for varying number of data symbols and investigation of achievable rate performance are left for our future studies. On the other hand, real time applications for CI-OFDM-RIQIM are considered as future work.

We hope that the schemes that we have proposed through this thesis might help the researchers working on waveform designs for next generation wireless communication systems.

BIBLIOGRAPHY

[Arslan et al., 2020] Arslan, E., Dogukan, A. T., and Basar, E. (Aug. 2020). Sparse-encoded codebook index modulation. *IEEE Trans. Veh. Technol.*, 69(8):9126–9130.

[Arslan et al., 2020] Arslan, E., Dogukan, A. T., and Basar, E. (Nov. 2020). Index modulation-based flexible non-orthogonal multiple access. *IEEE Wireless Commun. Lett.*, 9(11):1942–1946.

[Azim et al., 2020] Azim, A. W., Le Guennec, Y., Chafii, M., and Ros, L. (July 2020). Enhanced optical-OFDM with index and dual-mode modulation for optical wireless systems. *IEEE Access*, 8:128646–128664.

[Basar, 2016] Basar, E. (2016). Index modulation techniques for 5g wireless networks. *IEEE Communications Magazine*, 54(7):168–175.

[Başar, 2015] Başar, E. (Aug. 2015). OFDM with index modulation using coordinate interleaving. *IEEE Wireless Commun. Lett.*, 4(4):381–384.

[Basar, 2016] Basar, E. (Aug. 2016). On multiple-input multiple-output OFDM with index modulation for next generation wireless networks. *IEEE Trans. Signal Process.*, 64(15):3868–3878.

[Başar et al., 2013] Başar, E., Aygölü, Ü., Panayırcı, E., and Poor, H. V. (Nov. 2013). Orthogonal frequency division multiplexing with index modulation. *IEEE Trans. Signal Process.*, 61(22):5536–5549.

[Başar and Panayırcı, 2015] Başar, E. and Panayırcı, E. (Sep. 2015). Optical OFDM with index modulation for visible light communications. In *Proc. IEEE Int. Workshops Opt. Wireless Commun.*, pages 11–15. IEEE.

[Chen and Zheng, 2018] Chen, R. and Zheng, J. (Oct. 2018). Index-modulated MIMO-OFDM: Joint space-frequency signal design and linear precoding in rapidly time-varying channels. *IEEE Trans. Wireless Commun.*, 17(10):7067–7079.

[Chen et al., 2020] Chen, X., Wen, M., and Dang, S. (Sept. 2020). On the performance of cooperative OFDM-NOMA system with index modulation. *IEEE Wireless Commun. Lett.*, 9(9):1346–1350.

[Choi, 2017] Choi, J. (July 2017). Coded OFDM-IM with transmit diversity. *IEEE Trans. Commun.*, 65(7):3164–3171.

[Doğan et al., 2019] Doğan, S., Tusha, A., and Arslan, H. (Oct. 2019). NOMA with index modulation for uplink URLLC through grant-free access. *IEEE J. Sel. Topics Signal Process.*, 13(6):1249–1257.

[Dogukan and Basar, 2020] Dogukan, A. and Basar, E. (Oct. 2020). Orthogonal frequency division multiplexing with power distribution index modulation. *Electron. Lett*, 56(21):1156–1159.

[Dogukan and Basar, 2020] Dogukan, A. T. and Basar, E. (Nov. 2020). Super-mode OFDM with index modulation. *IEEE Trans. Wireless Commun.*, 19(11):7353–7362.

[Fan et al., 2014] Fan, R., Yu, Y. J., and Guan, Y. L. (Dec. 2014). Orthogonal frequency division multiplexing with generalized index modulation. In *Proc. IEEE Glob. Commun. Conf.*, pages 3880–3885. IEEE.

[Jaradat et al., 2018] Jaradat, A. M., Hamamreh, J. M., and Arslan, H. (Dec. 2018). OFDM with subcarrier number modulation. *IEEE Wireless Commun. Lett.*, 7(6):914–917.

[Jaradat et al., 2020] Jaradat, A. M., Hamamreh, J. M., and Arslan, H. (Mar. 2020). OFDM with hybrid number and index modulation. *IEEE Access*, 8:55042–55053.

[Khan and Rajan, 2006] Khan, M. Z. and Rajan, B. S. (May 2006). Single-symbol maximum likelihood decodable linear STBCs. *IEEE Trans. Inf. Theory*, 52(5):2062–2091.

[Le et al., 2021] Le, T. T. H., Tran, X. N., Ngo, V.-D., and Le, M.-T. (Sept. 2021). Repeated index modulation-OFDM with coordinate interleaving: Performance optimization and low-complexity detectors. *IEEE Syst. J.*, 15(3):3673–3681.

[Lu et al., 2018] Lu, S., Hemadeh, I. A., El-Hajjar, M., and Hanzo, L. (July 2018). Compressed-sensing-aided space-time frequency index modulation. *IEEE Trans. Veh. Technol.*, 67(7):6259–6271.

[Mao et al., 2016] Mao, T., Wang, Q., and Wang, Z. (Apr. 2016). Generalized dual-mode index modulation aided OFDM. *IEEE Commun. Lett.*, 21(4):761–764.

[Mao et al., 2018] Mao, T., Wang, Q., Wang, Z., and Chen, S. (1st Quart., 2018). Novel index modulation techniques: A survey. *IEEE Commun. Surv. Tuts.*, 21(1):315–348.

[Mao et al., 2016] Mao, T., Wang, Z., Wang, Q., Chen, S., and Hanzo, L. (Aug. 2016). Dual-mode index modulation aided OFDM. *IEEE Access*, 5:50–60.

[Şahin and Arslan, 2020] Şahin, M. M. and Arslan, H. (2020). Waveform-domain NOMA: The future of multiple access. In *Proc. IEEE Int. Conf. Commun. Workshops (ICC Workshops)*, pages 1–6. IEEE.

[Sahin et al., 2021] Sahin, M. M., Erol, I. G., Arslan, E., Basar, E., and Arslan, H. (Aug. 2021). OFDM-IM for joint communication and radar-sensing: a promising waveform for dual functionality. *Front. Commun. and Netw.*, page 34.

[Sasamori et al., 2011] Sasamori, F., Jia, Z., Handa, S., and Oshita, S. (2011). Performance analysis of repetition coded ofdm systems with diversity combining and higher-level modulation. *IEICE Trans. Commun.*, 94(1):194–202.

[Singleton, 1964] Singleton, R. (1964). Maximum distance q-nary codes. *IEEE Trans. Inf. Theory*, 10(2):116–118.

[Thanh et al., 2018] Thanh, H. L. T., Ngo, V.-D., Le, M.-T., and Tran, X. N. (2018). Repeated index modulation with coordinate interleaved OFDM. In *Proc. 5th NAFOSTED Conf. Infor. and Comput. Sci.*, pages 114–118. IEEE.

[Tusha et al., 2020] Tusha, A., Doğan, S., and Arslan, H. (Mar. 2020). A hybrid downlink NOMA with OFDM and OFDM-IM for beyond 5G wireless networks. *IEEE Signal Process. Lett.*, 27:491–495.

[Van Luong et al., 2018] Van Luong, T., Ko, Y., and Choi, J. (June 2018). Repeated MCIK-OFDM with enhanced transmit diversity under CSI uncertainty. *IEEE Trans. Wireless Commun.*, 17(6):4079–4088.

[Wang, 2021] Wang, L. (Sept. 2021). Generalized quadrature space-frequency index modulation for MIMO-OFDM systems. *IEEE Trans. Commun.*, 69(9):6375–6389.

[Wen et al., 2017] Wen, M., Basar, E., Li, Q., Zheng, B., and Zhang, M. (Sept. 2017). Multiple-mode orthogonal frequency division multiplexing with index modulation. *IEEE Trans. Commun.*, 65(9):3892–3906.

[Wen et al., 2018] Wen, M., Li, Q., Basar, E., and Zhang, W. (Oct. 2018). Generalized multiple-mode OFDM with index modulation. *IEEE Trans. Wireless Commun.*, 17(10):6531–6543.

[Xiao et al., 2014] Xiao, Y., Wang, S., Dan, L., Lei, X., Yang, P., and Xiang, W. (Aug. 2014). OFDM with interleaved subcarrier-index modulation. *IEEE Commun. Lett.*, 18(8):1447–1450.

[Yarkin and Coon, 2022] Yarkin, F. and Coon, J. P. (Jan 2022). Modulation based on a simple MDS code: Achieving better error performance than index modulation and related schemes. *IEEE Trans. Commun.*, 70(1):118–131.

[Yarkin and Coon, 2020] Yarkin, F. and Coon, J. P. (July 2020). Q-ary multi-mode OFDM with index modulation. *IEEE Wireless Commun. Lett.*, 9(7):1110–1114.

[Yarkin and Coon, 2020] Yarkin, F. and Coon, J. P. (Nov. 2020). Set partition modulation. *IEEE Trans. Wireless Commun.*, 19(11):7557–7570.

[Zheng et al., 2015] Zheng, B., Chen, F., Wen, M., Ji, F., Yu, H., and Liu, Y. (Nov. 2015). Low-complexity ML detector and performance analysis for OFDM with in-phase/quadrature index modulation. *IEEE Commun. Lett.*, 19(11):1893–1896.

[Zheng and Chen, 2017] Zheng, J. and Chen, R. (May 2017). Achieving transmit diversity in OFDM-IM by utilizing multiple signal constellations. *IEEE Access*, 5:8978–8988.